Sensor Configuration and Activation for Field Detection in Large Sensor Arrays

Youngchul Sung, *Member, IEEE*, Xin Zhang, *Member, IEEE*, Lang Tong, *Fellow, IEEE*, and H. Vincent Poor, *Fellow, IEEE*

***Abstract*—The problem of sensor configuration for the detection of correlated random fields using large sensor arrays is considered. Using error exponents that characterize the asymptotic behavior of the optimal detector, the detection performance of different sensor configurations is analyzed and compared. The dependence of the optimal configuration on parameters such as sensor signal-to-noise ratio (SNR), field correlation, etc., is examined, yielding insights into the most effective choices for sensor selection in various operating conditions. Simulation results validate the analysis based on asymptotic results for finite sample cases.**

***Index Terms*—Correlated signal, error exponent, Gauss–Markov field, Neyman–Pearson detection, optimal sampling, sensor configuration.**

I. Introduction

In this paper, we consider optimal sensor configuration or selection for densely deployed sensor networks for the detection of correlated random fields. An example in which the problem of such sensor selection arises is Sensor Network with Mobile Access (SENMA), where a mobile interrogator collects sensor data controlling sensor transmissions in the reachback channel. Due to limitations of sensor batteries, one of the main constraints for such a sensor network is energy efficiency. In the context of the considered detection problem, this implies that one should minimize the required amount of sensor data by selecting and activating sensors judiciously for a desired detection performance to maximize the lifetime of the network, since the number of activated sensors is directly related to the energy consumption of the entire network.

Manuscript received December 3, 2006; revised June 1, 2007. The associate editor coordinating the review of this manuscript and approving it for publication was Dr. Hongbin Li. This work was supported in part by the Army Research Office under Grant ARO-W911NF-06-1-0346 and the National Science Foundation under Contract CNS-0435190. The work of X. Zhang and H. V. Poor was also supported in part by the Air Force Research Laboratory under Cooperative Agreement FA8750-06-1-0252 and the Defense Advanced Research Projects Agency under Grant HR0011-06-1-0052. The work of Y. Sung was also supported in part by Brain Korea 21 Project, the School of Information Technology, KAIST.

Y. Sung is with Department of Electrical Engineering, Korea Advanced Institute of Science and Technology (KAIST), Daejeon 305-701, Korea (e-mail: ysung@ee.kaist.ac.kr).

X. Zhang is with the United Technologies Research Center, East Hartford, CT 06108 USA (e-mail: zhangx@utrc.utc.com).

L. Tong is with the School of Electrical and Computer Engineering, Cornell University, Ithaca, NY 14853 USA (e-mail: ltong@ece.cornell.edu).

H. V. Poor is with Department of Electrical Engineering, Princeton University, Princeton, NJ 08544 USA (e-mail: poor@princeton.edu).

Color versions of one or more of the figures in this paper are available online at http://ieeexplore.ieee.org.

Digital Object Identifier 10.1109/TSP.2007.907859

To simplify the problem for analysis and get insights into optimal sensor configuration, we focus on a 1-D space and examine how various parameters such as the field correlation, signal-to-noise ratio (SNR), etc., affect the optimal sensor configuration. We assume that each activated sensor takes a measurement of the field at its location, and subsequently transmits the data to the collector or fusion center, and the fusion center makes the final decision. We adopt the Neyman–Pearson formulation of fixing the detector size α and minimizing the miss probability. The miss probability P_M ($\mathcal{X}$, n; α, SNR, field correlation) is a function of the number n and locations $\mathcal{X} = \{x_1, \cdots, x_n\}$ of the activated sensors as well as detector size α, SNR, and field correlation. However, the exact miss probability in the correlated signal case is not available in general [1]. Our approach to this problem is based on the *error exponent*. Usually, the miss probability decreases exponentially as n increases, and the error exponent is defined as the corresponding decay rate

$$K(\mathcal{X};\, \alpha,\, \text{SNR}, \text{field correlation}) = -\lim_{n\to\infty} \frac{1}{n} \log P_M(\mathcal{X}, n; \alpha, \text{SNR}, \text{field correlation}). \quad (1)$$

The error exponent is a good performance index since it gives an estimate of the number of sensors required for a given detection performance; larger decay rate implies that fewer sensors are needed for a given miss probability. Hence, the optimal configuration problem can be formulated to find the best sensor locations $\mathcal{X}$ (where data should be collected) maximizing the error exponent for given α, SNR, and field correlation when the number of sensors is sufficiently large.

Based on our previous results on the behavior of the error exponent for the detection of correlated random fields [2], we investigate several strategies for sensor configuration for the detection problem, and propose guidelines for the optimal configuration for different operating regimes. (Introductory results were presented in [3].) Specifically, we consider uniform configuration, uniform configuration with random perturbation in location, periodic clustering, and periodic configuration with arbitrary sensor locations within a period. We show that the optimal configuration is a function of the SNR of the observations and the field correlation. For uniform configuration, the optimal strategy is to cover the entire signal field with the activated sensors for $\text{SNR} \geq 1$. For $\text{SNR} < 1$, on the other hand, there exists an optimal spacing between the activated sensors. We also derive the error exponents of periodic clustering and arbitrary periodic configurations in closed form by extending our previous results. These new expressions for error exponents reveal

the advantages and disadvantages of clustering of sensor observations for different operating condition. We compared the relative performance of the clustering to the uniform configuration using the asymptotic relative efficiency. It is shown that periodic clustering outperforms the uniform configuration depending on the field correlation and SNR. Furthermore, there exists an optimal cluster size for intermediate values of field correlation. The closed-form error exponent obtained for the vector state-space model explains the transitory error behavior for different sensor configurations as the field correlation changes. It is seen that the optimal periodic configuration is either periodic clustering or uniform configuration for highly correlated or almost independent signal fields. Monte Carlo simulations were performed, and simulation results validate our analysis based on asymptotic results in cases involving finitely many sensors.

A. Related Work

The detection of Gauss–Markov processes in Gaussian noise has been widely investigated. See [4] and references therein. There is also an extensive literature on the large deviations approach to the detection of Gaussian processes [5]–[11]. In particular, the works of Bahr and Bucklew [6], [7] are closest to our results. Their work concerns the Bayesian detection of Gaussian processes in which the threshold for the normalized log-likelihood ratio (LLR) is fixed and the Gärtner–Ellis theorem and Toeplitz distribution theorem can be applied. Using the Gärtner–Ellis theorem, they optimized the error exponent numerically and showed that the optimal sampling depends on SNR for a specific signal model. However, our work is based on the Neyman–Pearson formulation with a fixed size, in which the detection threshold varies with the number of samples and the Gärtner–Ellis theorem is not directly applicable. Under the Neyman–Pearson formulation, the error exponent is given by the almost-sure limit of the Kullback–Leibler rate (or relative entropy rate) [12]. Our work and extensions here are based on the large deviations results in [2], where the closed-form error exponent was derived for the Neyman–Pearson detection, with a fixed size, of correlated Gaussian signals using the innovations representation of the LLR [13]. The application of the large deviations principle (LDP) to sensor networks has been considered by other authors as well. Chamberland and Veeravalli have also considered the detection of correlated fields in large sensor networks under the formulation of LDP and a fixed threshold for the LLR test focusing on detection performance under power constraint [14].

B. Notation

The notation is standard. Vectors and matrices are written in boldface with matrices in capitals. For a matrix $\mathbf{A}$, $\mathbf{A}^T$ indicates the transpose, $\mathbf{A}(i,j)$ represents the element in the ith row and jth column, and $\det(\mathbf{A})$ and $\mathrm{tr}(\mathbf{A})$ represent the determinant and trace of $\mathbf{A}$, respectively. We reserve $\mathbf{I}_m$ for the identity matrix of size m (the subscript is included only when necessary). $\mathrm{diag}(\mathbf{X}_1,\ldots,\mathbf{X}_N)$ is a block diagonal matrix with $\mathbf{X}_1,\ldots,\mathbf{X}_N$ as its diagonal blocks. For a random vector $\mathbf{x}$, $\mathbb{E}\{\mathbf{x}\}$ is the statistical expectation of $\mathbf{x}$. The notation $\mathbf{x}\sim\mathcal{N}(\boldsymbol{\mu},\boldsymbol{\Sigma})$ means that $\mathbf{x}$ has the Gaussian distribution with mean $\boldsymbol{\mu}$ and covariance $\boldsymbol{\Sigma}$.

II. Data Model

We consider the detection of a stochastic signal $s(x)$ using n sensors deployed over 1-D space $\mathcal{X}=\{x: x\geq 0\}$. We assume that the underlying signal $s(x)$ is correlated over space and model it as the stationary solution of the stochastic differential equation

$$\frac{ds(x)}{dx}=-As(x)+Bu(x),\quad x\geq 0 \tag{2}$$

where the constants $A\geq 0$ and $B\in\mathbb{R}$ are known, and the initial condition is given by $s(0)\sim\mathcal{N}(0,\Pi_0)$. The input process $u(x)$ is a zero-mean unit-variance white Gaussian process, independent of both the initial state $s(0)$ and sensor measurement noises $\{w_i\}$.

We assume that each activated sensor measures the field at its location, and subsequently transmits the data to the fusion center, where a final decision is made.[1] The observation y_i from the activated sensor i located at x_i $(x_i<x_{i+1})$ is described by the following hypotheses:

$$\begin{cases} H_0: y_i=w_i, \\ H_1: y_i=s_i+w_i, \quad i=1,2,\cdots,n \end{cases} \tag{3}$$

where $\{w_i\}$ are independent and identically distributed (i.i.d.) sensor measurement noises drawn from $\mathcal{N}(0,\sigma^2)$ with a variance σ^2, and s_i is the spatial signal sample of the underlying signal $s(x)$ taken by sensor i, i.e., $s_i\triangleq s(x_i)$, as shown in Fig. 1. The dynamics of signal samples s_i at locations x_i are given by

$$\begin{aligned} s_{i+1}&=a_i s_i+u_i \\ a_i&=e^{-A\Delta_{i,i+1}} \end{aligned} \tag{4}$$

where $\Delta_{i,j}\triangleq|x_j-x_i|$ is the distance between sensor i and j, and the mean and variance of process noise u_i are given by $\mathbb{E}\{u_i\}=0$, $Q_i\triangleq\mathrm{Var}(u_i)=\Pi_0(1-a_i^2)$ for all i. Notice that $0\leq a_i\leq 1$ for $0\leq A\leq\infty$. (A similar model was also derived in [15].) From the stationarity, the SNR is given by

$$\mathrm{SNR}=\frac{\Pi_0}{\sigma^2}. \tag{5}$$

The hypotheses for the discrete model sampled by sensors can be written in vector form as

$$\begin{cases} H_0: \mathbf{y}_n=\mathbf{w}_n \\ H_1: \mathbf{y}_n=\mathbf{s}_n+\mathbf{w}_n \end{cases} \tag{6}$$

[1]We will not focus on local quantization of the measurement at the sensor level here, nor will we consider the transmission error to the fusion center. These are important design issues that should be treated separately.

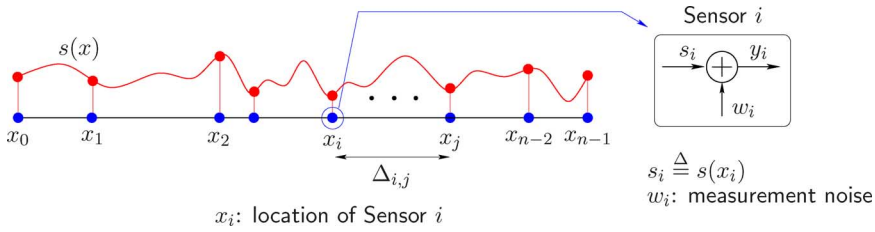

Fig. 1. Signal and measurement model.

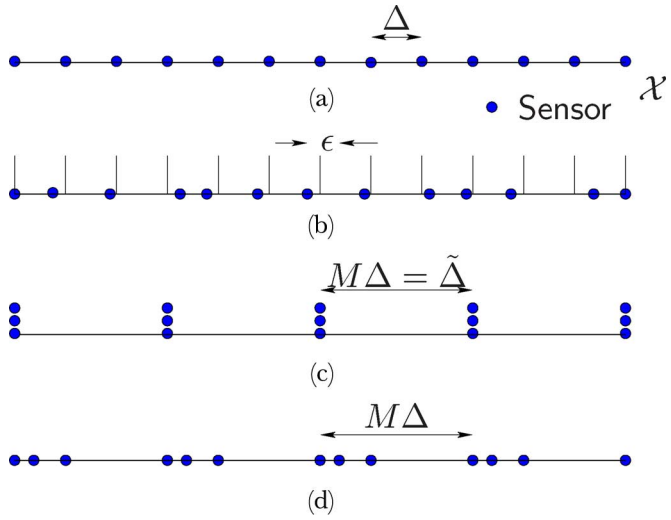

Fig. 2. Configurations for n sensor activations: (a) uniform configuration; (b) uniform configuration with random perturbation; (c) periodic clustering; and (d) arbitrary periodic configuration.

where $\mathbf{s}_n \triangleq [s_1, s_2, \cdots, s_n]^T$, $\mathbf{y}_n \triangleq [y_1, \cdots, y_n]^T$ and $\mathbf{w}_n \triangleq [w_1, \cdots, w_n]^T$. The noise vector $\mathbf{w}_n \sim \mathcal{N}(\mathbf{0}, \sigma^2\mathbf{I})$, and $\mathbf{s}_n \sim \mathcal{N}(\mathbf{0}, \mathbf{\Sigma}_{s,n})$ with $\mathbf{\Sigma}_{s,n}(i,j) = \Pi_0 \exp(-A\Delta_{i,j})$. Note that the covariance matrix $\mathbf{\Sigma}_{s,n}$ is not Toeplitz in general. Hence, $\mathbf{y}_n$ has the distribution $\mathcal{N}(0, \mathbf{\Sigma}_{0,n})$ and $\mathcal{N}(0, \mathbf{\Sigma}_{1,n})$, where $\mathbf{\Sigma}_{0,n} = \sigma^2\mathbf{I}$ and $\mathbf{\Sigma}_{1,n} = \mathbf{\Sigma}_{s,n} + \sigma^2\mathbf{I}$, under H_0 and H_1, respectively.

III. Sensor Configuration and Error Exponent

In this section, we consider several sensor configurations, i.e., the design of $\mathcal{X} = \{x_1, \cdots, x_n\}$ in the space, and investigate the corresponding detection performance of each via the error exponent. We also present the closed-form error exponent for several configuration cases by extending our previous results in [2]. Specifically, we consider the uniform configuration, uniform configuration with random perturbation, clustering, and periodic configuration with arbitrary locations within a spatial period, as described in Fig. 2. We provide the optimal configuration for the uniform configuration for the detection performance and examine the benefits of other configurations. The error exponent for the uniform configuration with random perturbation in sensor location is not obtained in the paper, and the performance in this case is studied via simulations. However, it is possible to derive the error exponent when the sensor spacings are i.i.d. random variables using the generalized strong law of large numbers (SLLN).

A. Uniform Configuration

The error exponent of the Neyman–Pearson detection of the hypotheses (3) is given by the asymptotic Kullback–Leibler rate defined as the almost-sure limit of $(1/n)\log(p_{0,n}/p_{1,n})(y_1, \cdots, y_n)$ as $n \to \infty$ under $p_{0,n}$, where $p_{0,1}$ and $p_{1,n}$ are the joint probability density of $\{y_1, y_2, \cdots, y_n\}$ under H_0 and H_1, respectively.

In the case of uniformly located sensors with spacing Δ between two neighboring sensors, the signal dynamics are given by a linear invariant state-space model (4) with

$$a_i = a = e^{-A\Delta} \text{ and } Q_i = Q = \Pi_0(1-a^2) \text{ for all } i \quad (7)$$

and the covariance matrix $\mathbf{\Sigma}_{s,n}$ of the signal vector is a Toeplitz matrix of which the asymptotic eigenvalue distribution is known [16], [17]. Note that $a = 0$ and $a = 1$ correspond to the independent and the perfectly correlated sample cases, respectively.

In this case, the hypotheses are given by (3), (4), and (7), and the results in [2] apply directly. The error exponent is given by the following theorem from [2].

Theorem 1 (Error Exponent for the Uniform Case [2]): The error exponent for the Neyman–Pearson detection of the hypotheses (3), (4), (7) with a fixed size $\alpha \in (0,1)$ is given by

$$K = -\frac{1}{2}\log\frac{\sigma^2}{R_e} + \frac{1}{2}\frac{\tilde{R}_e}{R_e} - \frac{1}{2} \quad (8)$$

independently of the value of α, where R_e and $\tilde{R}_e$ are the steady-state variances of the innovations process of $\{y_i\}$ under H_1 and H_0, respectively. Specifically, R_e and $\tilde{R}_e$ are given by

$$R_e = \sigma^2 + P \quad (9)$$

and

$$\tilde{R}_e = \sigma^2\left(1 + \frac{a^2P^2}{P^2 + 2\sigma^2P + (1-a^2)\sigma^4}\right) \quad (10)$$

where

$$P = \frac{1}{2}\sqrt{[\sigma^2(1-a^2) - Q]^2 + 4\sigma^2Q} - \frac{1}{2}\sigma^2(1-a^2) + \frac{Q}{2}. \quad (11)$$

Here, P is the steady-state error variance of the minimum mean-square error (MMSE) estimator for the signal s_i.

Here, we note that the error exponent for the miss probability with a fixed size does not depend on the value α of the size. Thus, the error exponent depends only on sensor location $\mathcal{X}$ and SNR. It is shown in [2] that the error exponent K is monotone

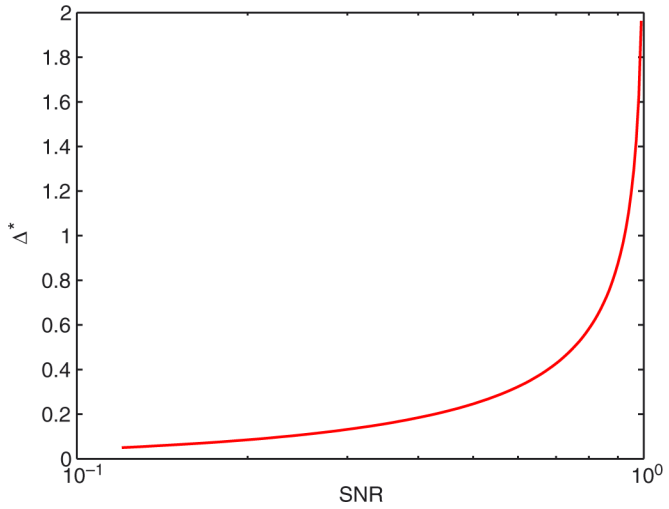

Fig. 3. Optimal spacing between sensors for infinite signal field ($\mathrm{SNR} < 1$, $A = 1$).

decreasing as the correlation coefficient a increases for a given SNR for $\mathrm{SNR} \geq 1$, whereas for $\mathrm{SNR} < 1$ there exists a nonzero correlation value a^* that maximizes K, and a^* is given by the solution of the following equation:

$$\left[1 + a^2 + \mathrm{SNR}(1 - a^2)\right]^2 - 2\left(\frac{R_e}{\sigma^2} + \frac{a^4\sigma^2}{R_e}\right) = 0. \quad (12)$$

Further, a^* converges to one as SNR approaches zero. It is also shown in [2] that the error exponent K increases monotonically as SNR increases for a given correlation coefficient $0 \leq a \leq 1$, and at high SNR the error exponent K increases as a function of SNR as

$$K \sim \frac{1}{2}\log(1 + \mathrm{SNR}). \quad (13)$$

The key connection between the sensor configuration and detector performance is given by the correlation coefficient $a = e^{-A\Delta}$. First, consider $\mathrm{SNR} \geq 1$. In this case, the detection performance degrades as the sample correlation increases (i.e., $a \uparrow 1$), and the sample correlation increases as the sensor spacing Δ decreases for a given field diffusion rate A in (2). Hence, when the support of the signal field $\mathcal{S}$ is finite and we have n sensors to activate in the field, the optimal uniform configuration is to distribute the n activated sensors to cover the entire support of the signal field, which makes the observations least correlated; localizing all the activated sensors in a subregion of the stationary random signal field is not optimal. For the detection of weak signals ($\mathrm{SNR} < 1$), on the other hand, the optimal spacing Δ^* for an infinite (in size) signal field is given by

$$\Delta^* = -\log\frac{a^*}{A} \quad (14)$$

where a^* is given by the solution of (12). The optimal spacing Δ^* is finite for any SNR strictly less than one. Fig. 3 shows the optimal spacing as a function of SNR is shown for $A = 1$.

For a finite-duration signal field $\mathcal{S}$ with n activated sensors, Δ^* is still optimal among the class of uniform configurations if the sensor coverage is less than the spatial field duration $|\mathcal{S}|$, i.e., $n\Delta^* \leq |\mathcal{S}|$. In this case, the sensor field does not need to cover the entire signal field. If $n\Delta^* > |\mathcal{S}|$, however, Δ^* may not be the optimal spacing any more. The error exponent decreases when the spacing Δ deviates from the optimal spacing Δ^*. Hence, activating sensors fewer than $n^* \triangleq \lfloor |\mathcal{S}|/\Delta^* \rfloor$ with spacing larger than Δ^* always yields a worse performance than n^* sensors with spacing Δ^*. However, this may not be the case for activating more sensors than n^* (up to n) with a reduced spacing from Δ^*. Although the error exponent decreases by reducing the spacing, i.e., per-sensor performance degrades, more sensors are activated over the signal field. Therefore, better performance is possible for the second case since the product of the error exponent and the number of samples determines the miss probability.

A similar situation also occurs at $\mathrm{SNR} \geq 1$ for a finite-duration signal field. In this case, the error exponent increases monotonically as the correlation decreases, as mentioned earlier. Hence, by spreading the activated sensors with a reduced number of activated sensors in the finite-duration signal field, sensor observations become less correlated and the slope of error decay per sensor sample becomes larger at a cost of reducing the number of observations. However, the increase in the error exponent is not sufficient to compensate for the loss in the number of sensors in the field. This is because the error exponent K is a concave monotone increasing function of Δ at high SNR, and hence $K(\gamma\Delta) \leq \gamma K(\Delta)$ for $\gamma > 1$. The monotonicity is simply seen from the monotonicity of K as a function of a and that of a as a function Δ. The concavity is also easily proved using the concavity of K as a function of a, i.e.,

$$\begin{aligned} &K\left(a\left(\beta\Delta_1 + (1-\beta)\Delta_2\right)\right) \\ &\quad \geq K\left(\beta a(\Delta_1) + (1-\beta)a(\Delta_2)\right), \\ &\quad \geq \beta K\left(a(\Delta_1)\right) + (1-\beta)K\left(a(\Delta_2)\right), \quad (0 \leq \beta \leq 1). \end{aligned}$$

The first inequality is because K is a monotone decreasing function of a and $a(\beta\Delta_1 + (1-\beta)\Delta_2) \leq \beta a(\Delta_1) + (1-\beta)a(\Delta_2)$ since $a(\Delta) = \exp(-A\Delta)$, and the second inequality is by the concavity of K as a function of a at high SNR. The error exponent K as a function of Δ at 10-dB SNR is shown in Fig. 4. Hence, when the maximum number of available sensors in a finite-duration signal field case is n, the optimal configuration is to activate all n sensors covering the entire field.

Another interesting fact about the finite-duration signal field is the asymptotic behavior when the number of sensors increases without bound. In this case, the correlation coefficient converges to one, i.e.,

$$a = \exp\left(-A\frac{|\mathcal{S}|}{n}\right) \to 1 \quad \text{as} \quad n \to \infty. \quad (15)$$

It is shown in [2] that the error probability does not decay exponentially when $a = 1$, but decays with polynomial order $n^{-1/2}$ for any finite A as $n \to \infty$. The exception is the singular case where $A = \infty$, i.e., the signal is a white process. Therefore, for the detection of stationary correlated fields, it is a better strategy

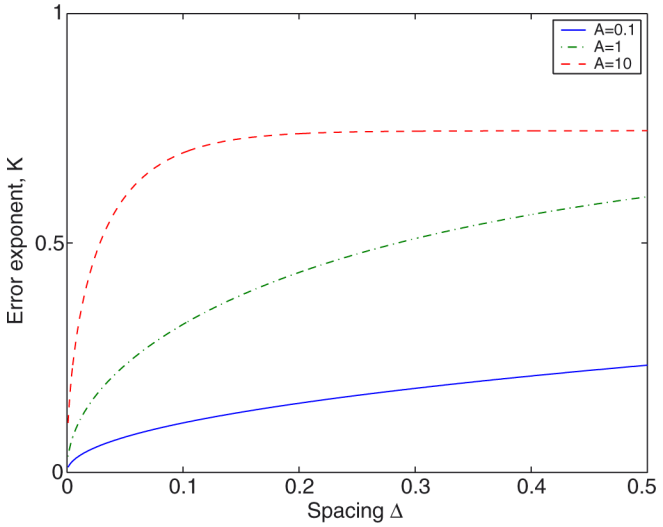

Fig. 4. Error exponent versus Δ (SNR $=$ 10 dB).

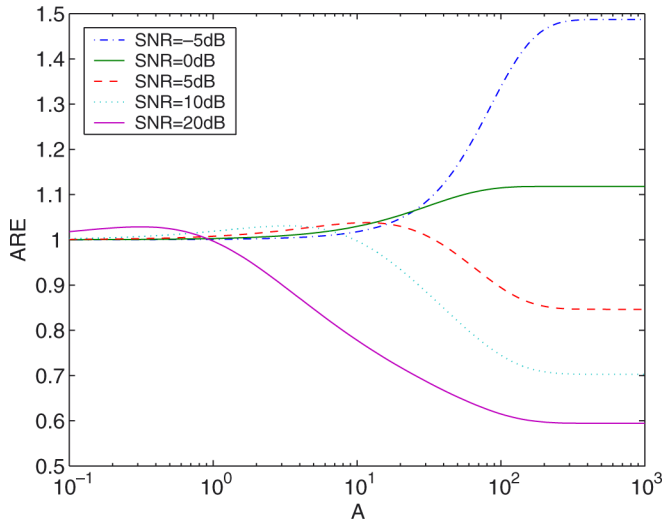

Fig. 5. Asymptotic relative efficiency versus diffusion rate ($M = 2$, $\Delta = 1/99$, SNR $= -5$, 0, 5, 10, 20 dB).

to cover a larger area as long as the signal field extends there than to localize activated sensors more densely in a subregion.

B. Periodic Clustering

The uniform configuration for a finite-duration signal field reveals that we have a benefit at high SNR by making sensor spacing large to obtain less correlated observations, but activating fewer sensors results in a bigger loss than the gain from samples' being less correlated. This leads to our next configuration: periodic clustering, as shown in Fig. 2(c), aiming at the benefits from both correlation and the number of activated sensors. In this configuration, we activate M sensors very close in location, and repeat this multiple activation periodically over the signal field. In this way, the spacing between clusters becomes larger than that of the uniform configuration while the number of activated sensors is preserved.

To simplify the analysis, we assume that the M sensors of a cluster are located at the same position. With the total number of activated sensors $n = MN$, the observation vector $\mathbf{y}_n = [y_1, y_2, \cdots, y_n]^T$ under H_1 is given by

$$\mathbf{y}_n = \tilde{\mathbf{s}}_n \otimes \mathbf{1}_M + \mathbf{w}_n \tag{16}$$

where $\otimes$ is the Kronecker product, $\mathbf{1}_M = [1, \cdots, 1]^T$, and $\tilde{\mathbf{s}}_n = [s(0), s(\tilde{\Delta}), \cdots, s(N\tilde{\Delta})]^T$ with $\tilde{\Delta} = M\Delta$. (Δ is the sensor spacing for the uniform configuration for n sensors in $\mathcal{X}$.) The covariance matrix of the observation vector is given by

$$\mathbb{E}\left\{\mathbf{y}_n \mathbf{y}_n^T\right\} = \begin{cases} \Sigma_{s,N}(\tilde{a}) \otimes \mathbf{1}_M \mathbf{1}_M^T + \sigma^2 \mathbf{I}, & \text{under } H_1 \\ \sigma^2 \mathbf{I}, & \text{under } H_0 \end{cases} \tag{17}$$

where $\tilde{a} = \exp(-A\tilde{\Delta})$. The signal covariance matrix has a block Toeplitz form due to the perfect correlation of signal samples within a cluster. $\mathbf{\Sigma}_{s,N}(\tilde{a})$ in (17) is a positive-semidefinite Toeplitz matrix of which the kth off-diagonal entries are given by $\tilde{r}_s(k) = \Pi_0 \tilde{a}^k$. For any $A > 0$ and finite $\tilde{\Delta}$, $\tilde{r}_s(\cdot)$ is an absolutely summable sequence; the eigenvalues of $\mathbf{\Sigma}_{s,n}$ are bounded from above and below [17]. Using the convergence of the eigenvalues of $\mathbf{\Sigma}_{s,N}$ and the properties of the Kronecker product, the error exponent for periodic clustering is obtained and given by the following proposition.

Proposition 1 (Periodic Clustering): For the Neyman–Pearson detector for the hypotheses (6) with level $\alpha \in (0, 1)$ and periodically clustered sensor configuration, the error exponent of the miss probability is given by

$$\tilde{K} = \frac{1}{M} K(\tilde{\Delta}; M * \mathrm{SNR}) \tag{18}$$

where $K(\tilde{\Delta}; M * \mathbf{SNR})$ is the error exponent in Theorem 1 for uniform configuration with spacing $\tilde{\Delta}$ and $M * \mathbf{SNR}$ for each sensor.

Proof: See the Appendix.

It is shown in the proof that the optimal detection for periodic clustering comprises two steps. We first take an average of the observations within each cluster and then apply optimal detection for a single sample at each location to the ensemble of N average values. Intuitively, it is reasonable to average the observations within a cluster since the signal component is aligned and the noise is random. By averaging, the magnitude of the signal component increases by M times with the increase in the accumulated noise power by the same factor. Thus, the SNR within a cluster increases by the factor M. This is shown in the form of the error exponent (18) for periodic clustering.

The error exponent (18) reveals the advantages and disadvantages of periodic clustering over a uniform configuration covering the same signal field. First, clustering provides two benefits. One is that the correlation between clusters is reduced for the same diffusion rate A by making the spacing larger, and the error decay per cluster increases for high SNR. Second, the SNR for each cluster increases by the factor M. However, the effective number of signal samples is also reduced by the same factor as compared with the uniform configuration. The performance of clustering is determined by the dominating factor depending

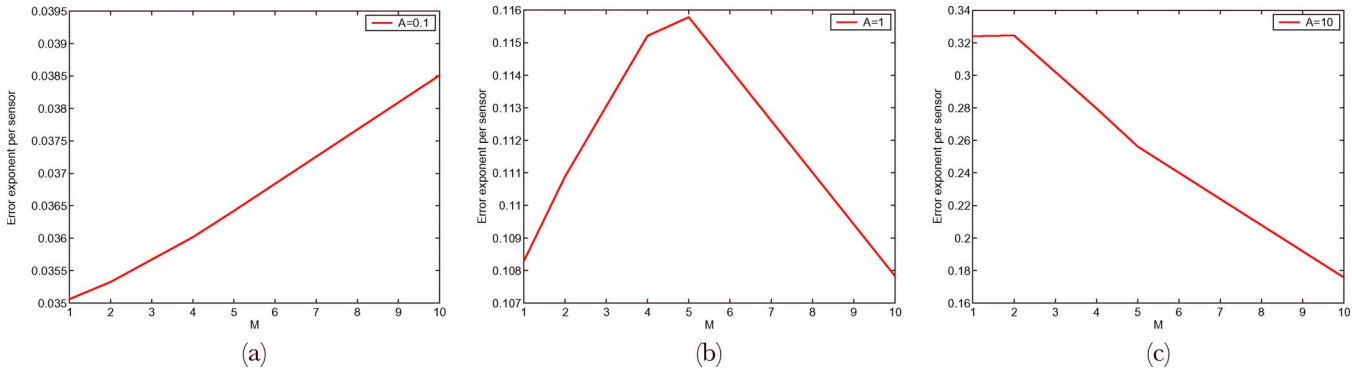

Fig. 6. $\tilde{K}$ versus M (SNR $= 10$ dB): (a) $A = 0.1$; (b) $A = 1$; and (c) $A = 10$.

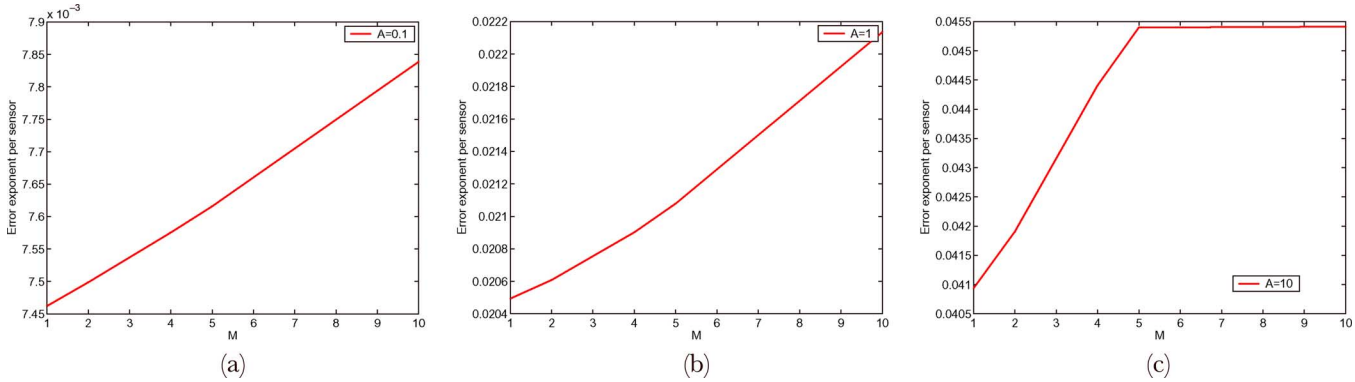

Fig. 7. $\tilde{K}$ versus M (SNR $= -3$ dB): (a) $A = 0.1$; (b) $A = 1$; and (c) $A = 10$.

on the diffusion rate A of the underlying signal and the SNR of the observations.

To get insight into the relative performance, in Fig. 5, we plot the asymptotic relative efficiency (ARE) defined as

$$\text{ARE} \triangleq \frac{\tilde{K}}{K} \tag{19}$$

for $M = 2$ and several different SNR values. The ARE is the ratio of the required number of samples of one scheme to that of the other when both have the same detection performance, and is a good measure of the relative performance between two detection schemes in the large sample regime. As shown in the figure, it is seen that clustering outperforms the uniform configuration for a wide range of the diffusion rate A at low SNR (SNR $= -5$ and 0 dB), whereas at high SNR (SNR $= 5$, 10, 20 dB) the clustering has worse performance than the uniform configuration when the field is weakly correlated. Notice that when the field is strongly correlated, the clustering yields better performance than the uniform configuration even at high SNR, but the performance difference between the clustering and the uniform configuration is not significant.

Now we consider different values of M. Fig. 6 shows the per-sensor error exponent $\tilde{K}$ for different diffusion rates at 10-dB SNR. The cluster size is chosen as $M = [1, 2, 4, 5, 10]$ to cover a field with length one with total $n = 100$ sensors. For the highly correlated field $(A = 0.1)$, it is observed that the reduced correlation between signal samples is the dominant factor and the clustering $(M > 1)$ gives better performance than the uniform configuration (i.e., $M = 1$). This is consistent to the result in [2] that the gain in the error exponent due to reducing the sample correlation is large in the strong correlation region (i.e., near $a = 1$). For the highly independent signal field $(A = 10)$, on the other hand, the clustering yields worse performance than the uniform configuration $(M = 1)$. In this case, the sample correlation between the activated sensors is already weak, and the increase in the error exponent due to increased spacing is insignificant in the region around $a = 0$. Hence, the benefit of clustering results mostly from the increase in SNR. By (13), however, the rate of increase in the error exponent due to the increased SNR is $(1/2) \log M$ at high SNR, which does not compensate for the loss in the number of effective samples by the factor $1/M$. For the signal field with intermediate correlation, there is a tradeoff between the gain and loss of clustering, and there exists an optimal cluster size as shown in Fig. 6(b).

Fig. 7 shows $\tilde{K}$ for periodic clustering for -3 dB-SNR with other parameters the same as those in the high SNR case. It is seen that periodic clustering outperforms the uniform configuration in all considered correlation values at -3-dB SNR, and the SNR is the dominant factor in the detector performance at low SNR.

Clustering also provides an intuitive explanation for the polynomial behavior of the asymptotic error decay rate for the infinite density model (15) that we considered in Section III-A. We can view an increase in the number n of sensors in a finite-size signal field as increasing the cluster size M with a fixed number N of clusters. As n increases with a fixed N, SNR per cluster increases linearly with n, and will be in the high SNR regime

eventually. At high SNR, the error exponent increases at the rate of $(1/2)\log(1+\mathrm{SNR})$ (13). Hence, the asymptotic behavior of the overall miss probability is given by

$$P_M \sim C\exp(-NK) \sim C_1 \exp\left(-\frac{1}{2}N\log n\right) = C_1 n^{-N/2} \tag{20}$$

for sufficiently large n. It is clear that in highly correlated cases the decay in the error probability with an increasing number of samples is mainly due to the noise averaging effect rather than the effect of the innovations contained in the observations.

C. Arbitrary Periodic Configuration

It is observed in the previous section that periodic clustering outperforms the uniform configuration depending on the field correlation. However, periodic clustering is limited since all the sensors within a spatial period are activated on the same location. Considering the periodic structure we now generalize the locations of the scheduled sensors within a period. We first provide a closed-form expression for the error exponent for the Neyman–Pearson detection of stationary vector Gauss–Markov processes using noisy observations. Using the closed-form error exponent, we then examine the optimal periodic configuration.

We again consider scheduling $n = MN$ sensors over $\mathcal{X}$ with M sensors within a period, and denote the relative distance of M sensors within a period as

$$x_1 = 0,\ x_2 - x_1 = \delta_1,\ x_3 - x_2 = \delta_2,\ \cdots, x_{M+1} - x_M = \delta_M.$$

Hence, the interval of a spatial period is $\Delta = \delta_1 + \cdots + \delta_M$. Define the signal and observation vectors for period i as

$$\vec{s}_i \triangleq [s_{1i}, s_{2i}, \cdots, s_{Mi}]^T, \quad i = 1, \cdots, N \tag{21}$$

$$\vec{y}_i \triangleq [y_{1i}, y_{2i}, \cdots, y_{Mi}]^T, \quad i = 1, \cdots, N \tag{22}$$

where $s_{mi} = s_{(i-1)M+m}$ and $y_{mi} = y_{(i-1)M+m}$. The hypotheses (3) can be rewritten in vector form as

$$\begin{aligned} H_0 &: \vec{y}_i = \vec{w}_i, \quad i = 1, 2, \cdots, N \\ H_1 &: \vec{y}_i = \vec{s}_i + \vec{w}_i, \quad i = 1, 2, \cdots, N \end{aligned} \tag{23}$$

where the measurement noise $\vec{w}_i \sim \mathcal{N}(\mathbf{0}, \sigma^2\mathbf{I}_M)$ independent over i, and the signal vector $\vec{s}_i$ satisfies the vector state-space model

$$\begin{aligned} &\vec{s}_{i+1} = \mathbf{A}\vec{s}_i + \mathbf{B}\vec{u}_i \\ &\vec{u}_i \overset{i.i.d.}{\sim} \mathcal{N}(0,\ \mathbf{Q}), \quad \mathbf{Q} \geq 0 \end{aligned} \tag{24}$$

where the process noise $\vec{u}_i \triangleq [u_{1i}, u_{2i}, \cdots, u_{Mi}]^T$. Specifically, the feedback and input matrices, $\mathbf{A}$ and $\mathbf{B}$, are given from the scalar state-space model (4) as

$$\mathbf{A} = \begin{bmatrix} 0 & 0 & 0 & e^{-A\delta_M} \\ 0 & 0 & 0 & e^{-A(\delta_M+\delta_1)} \\ 0 & 0 & 0 & \vdots \\ 0 & 0 & 0 & e^{-A(\delta_M+\delta_1+\cdots+\delta_{M-1})} \end{bmatrix}$$

$$\mathbf{B} = \begin{bmatrix} 1 & 0 & 0 & 0 \\ e^{-A\delta_1} & 1 & 0 & 0 \\ \vdots & \cdots & \ddots & 0 \\ e^{-A(\delta_1+\cdots+\delta_{M-1})} & & e^{-A\delta_{M-1}} & 1 \end{bmatrix} \tag{25}$$

and

$$\mathbf{Q} = \Pi_0 \mathrm{diag}\left((1-e^{-2A\delta_M}), (1-e^{-2A\delta_1}), \cdots, (1-e^{-2A\delta_{M-1}})\right).$$

Notice that $\mathbf{A}$, $\mathbf{B}$, and $\mathbf{Q}$ do not vary with i due to the periodicity[2] and only the last column of $\mathbf{A}$ is nonzero due to the Markov property of the scalar process $\{s_i\}$. The single nonzero eigenvalue of $\mathbf{A}$ corresponding to the last column is simply given by $\lambda = e^{-A\Delta}$ so that $|\lambda| < 1$ for arbitrary sensor locations within a period for any diffusion rate $A > 0$. Notice that the eigenvalue is the same as the correlation coefficient a with sampling distance Δ, the period of the spatial interval. The initial condition for the vector model is given by

$$\vec{s}_1 \sim \mathcal{N}(0, \mathbf{C}_0) \tag{26}$$

where $\mathbf{C}_0(i,j) = \Pi_0 e^{-A\Delta_{i,j}}$, $i, j = 1, 2, \cdots, M$. The initial covariance matrix $\mathbf{C}_0$ is derived from the scalar initial condition $s_1 \sim \mathcal{N}(0, \Pi_0)$, and satisfies the following Lyapunov equation:

$$\mathbf{C}_0 = \mathbf{A}\mathbf{C}_0\mathbf{A}^T + \mathbf{B}\mathbf{Q}\mathbf{B}^T. \tag{27}$$

Thus, the vector signal sequence $\{\vec{s}_i\}$ is a stationary process although the scalar process is not in general for the arbitrary periodic configuration.

Generalizing the results in [2], we provide a closed-form expression for the error exponent of the Neyman–Pearson detection of stationary vector processes with noisy observations in the following proposition.

Proposition 2 (Arbitrary Periodic Configuration): For the Neyman–Pearson detection for the hypotheses (23) and (24) with level $\alpha \in (0,1)$ (i.e., $P_F \leq \alpha$), the error exponent of the miss probability (per a vector observation) is given by

$$K_v = -\frac{1}{2}\log\frac{\sigma^{2M}}{\det(\mathbf{R}_e)} + \frac{1}{2}\mathrm{tr}\left(\mathbf{R}_e^{-1}\tilde{\mathbf{R}}_e\right) - \frac{M}{2} \tag{28}$$

independently of the value of α. The steady-state covariance matrices $\mathbf{R}_e$ and $\tilde{\mathbf{R}}_e$ of the innovation process calculated under H_1 and H_0, respectively, are given by

$$\mathbf{R}_e = \sigma^2\mathbf{I}_M + \mathbf{P} \tag{29}$$

where $\mathbf{P}$ is the unique stabilizing solution of the discrete-time Riccati equation

$$\mathbf{P} = \mathbf{A}\mathbf{P}\mathbf{A}^T + \mathbf{B}\mathbf{Q}\mathbf{B}^T - \mathbf{A}\mathbf{P}\mathbf{R}_e^{-1}\mathbf{P}\mathbf{A}^T \tag{30}$$

and

$$\tilde{\mathbf{R}}_e = \sigma^2(\mathbf{I}_M + \tilde{\mathbf{P}}) \tag{31}$$

[2]We have a "time"-invariant vector state-space model (24) from a "time"-varying scalar state-space model (4). This makes it possible to derive the error exponent for the arbitrary periodic configuration.

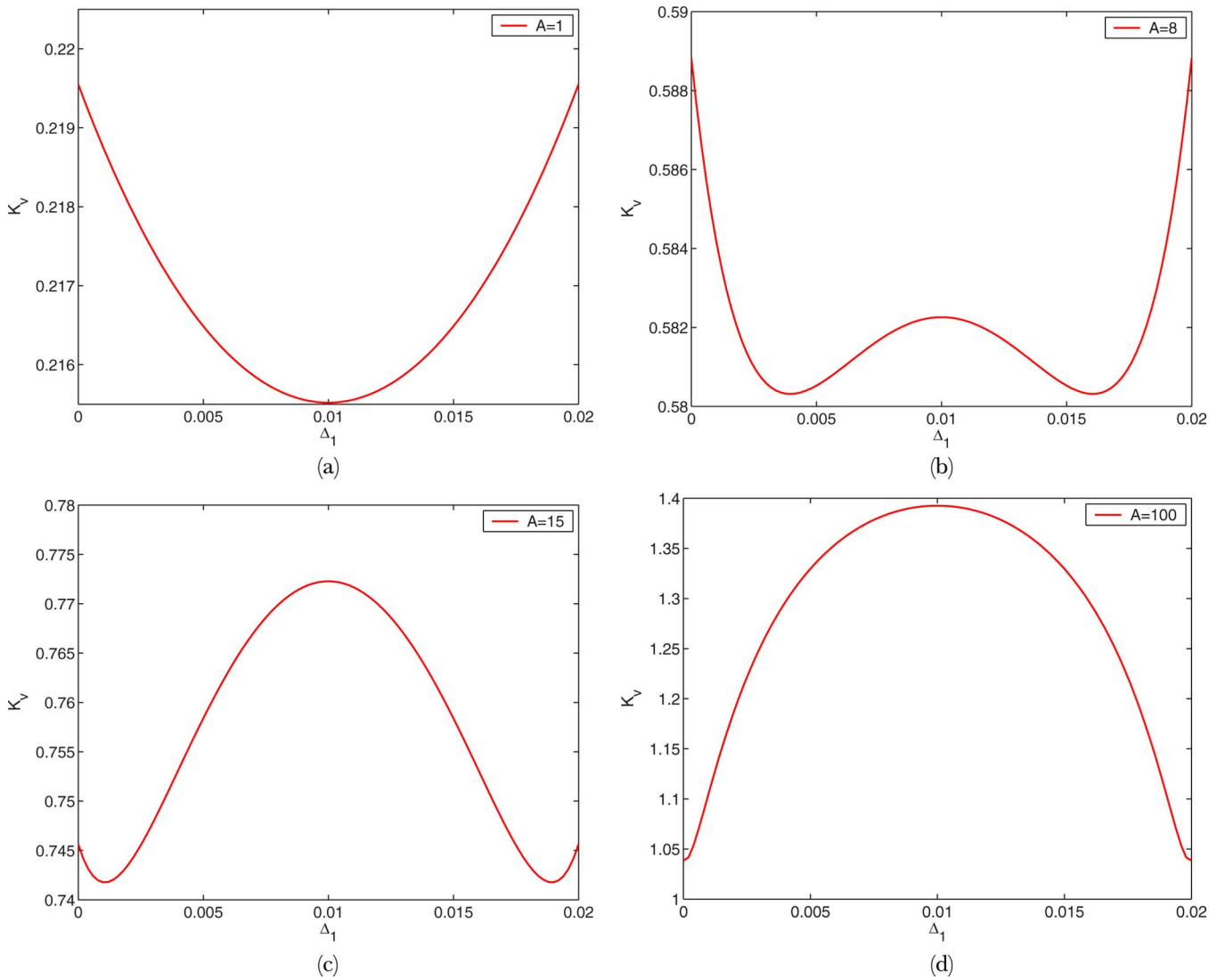

Fig. 8. K_v versus Δ_1 ($M = 2, \Delta = 0.02, \mathrm{SNR} = 10$ dB): (a) $A = 1$; (b) $A = 8$; (c) $A = 15$; and (d) $A = 100$.

where $\tilde{\mathbf{P}}$ is the unique positive-semidefinite solution of the following Lyapunov equation:

$$\tilde{\mathbf{P}} = (\mathbf{A} - \mathbf{K}_p)\tilde{\mathbf{P}}(\mathbf{A} - \mathbf{K}_p)^T + \mathbf{K}_p\mathbf{K}_p^T \tag{32}$$

and $\mathbf{K}_p = \mathbf{A}\mathbf{P}\mathbf{R}_e^{-1}$.

Proof: See the Appendix.

Using (28), we now examine the large sample performance for the detection of correlated fields using sensors with arbitrary periodic configuration and explain the transitory behavior of optimal configuration as the field correlation changes. First, we consider the case of $M = 2$, which provides insights into the detection problem. In this case, we have the freedom to schedule one intermediate sensor at an arbitrary location within an interval Δ. Periodic clustering and uniform configuration are special cases of this configuration with $\Delta_1 = 0$ and $\Delta_1 = \Delta/2$, respectively. Fig. 8 shows the error exponent for different diffusion rates at $\mathrm{SNR} = 10$ dB. We observe an interesting behavior with regard to the diffusion rate. For the highly correlated case ($A = 1$), periodic clustering ($\Delta_1 = 0$) yields the best performance and the uniform configuration provides the worst. As the field correlation becomes weak ($A = 8$), however, we observe that a second lobe grows at the uniform configuration point ($\Delta_1 = \Delta/2$). The value of the second lobe becomes larger than that of the clustering as the correlation becomes weaker ($A = 15$), and eventually the error exponent decreases monotonically as the configuration deviates from uniform configuration to periodic clustering. This behavior of the error exponent clearly shows that the optimal configuration is dependent on the field correlation. One should reduce the correlation between observations for highly correlated fields whereas the uniform configuration is best for almost independent signal fields, which is consistent with the results in the previous sections. Interestingly, it is seen that the optimal configuration for $M = 2$ at high SNR is either clustering or the uniform configuration depending on the field correlation; no configuration in-between is optimal! Fig. 9 shows the error exponent for $M = 2$ at $\mathrm{SNR} = -3$ dB. It is seen that clustering is always the best strategy for all values of the field correlation considered and the increase in the effective

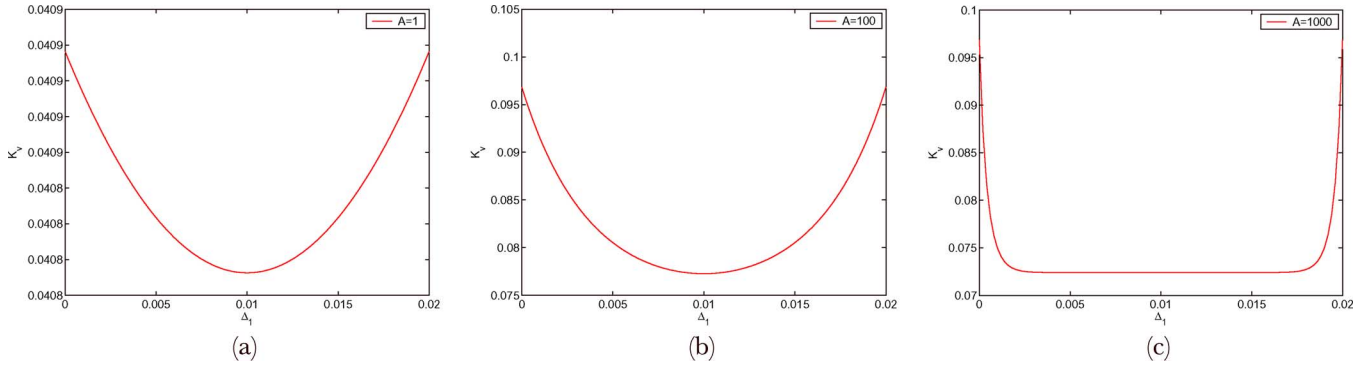

Fig. 9. K_v versus Δ_1 ($M = 2$, $\Delta = 0.02$, SNR $= -3$ dB): (a) $A = 1$ (b) $A = 100$ (c) $A = 1000$.

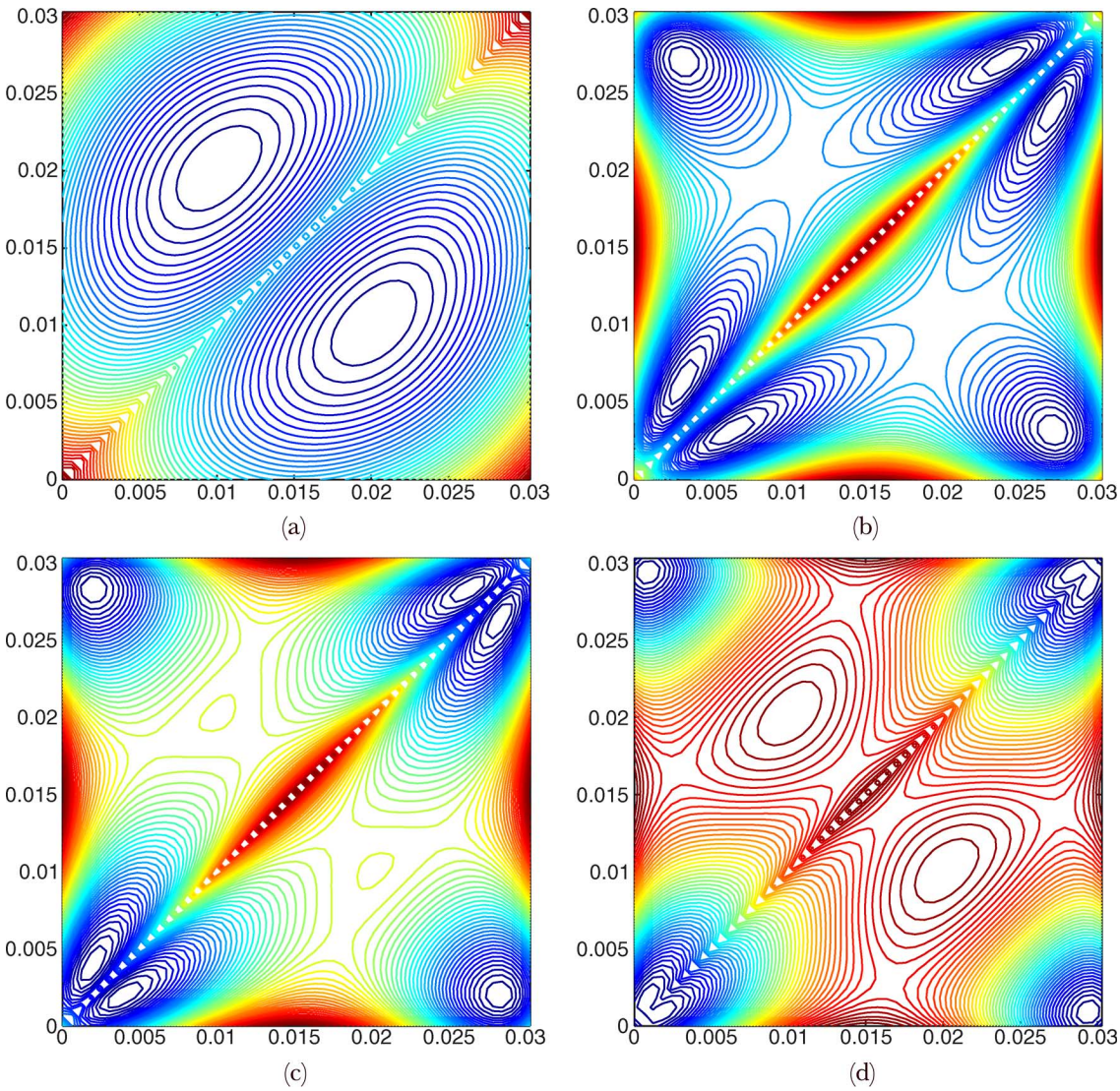

Fig. 10. K_v versus (x_2, x_3) ($M = 3$, $\Delta = 0.03$, SNR $= 10$ dB): (a) $A = 1$; (b) $A = 5$; (c) $A = 6$; and (d) $A = 9$ (red: high value; blue: low value).

SNR due to noise averaging is the dominant factor in the detection performance at low SNR. It is also observed that the location of the intermediate sensor is not important for the almost independent field $(A = 1000)$ unless it is very close to the first sensor within a period. This is intuitively obvious since the intermediate sensor provides an almost independent observation (for which the location does not matter) as it separates from the first and the noise averaging is not available between the independent samples.

In the case of $M = 3$, the location of one sensor in a period is fixed and we can choose the locations (x_2, x_3) of the two other sensors arbitrarily such that $0 \leq x_2 \leq \Delta$ and $0 \leq x_3 \leq \Delta$. Fig. 10 shows the error exponent as a function of (x_2, x_3) for $M = 3$ at 10-dB SNR. Similar behavior to the case of

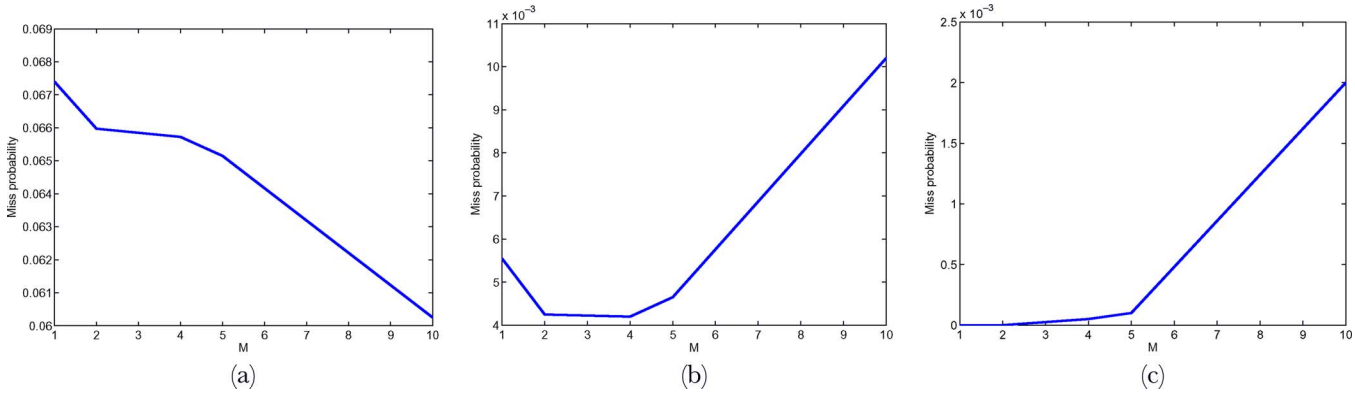

Fig. 11. P_M versus M ($|\mathcal{S}| = 1$, SNR $= 10$ dB): (a) $A = 0.1$; (b) $A = 1$; and (c) $A = 10$.

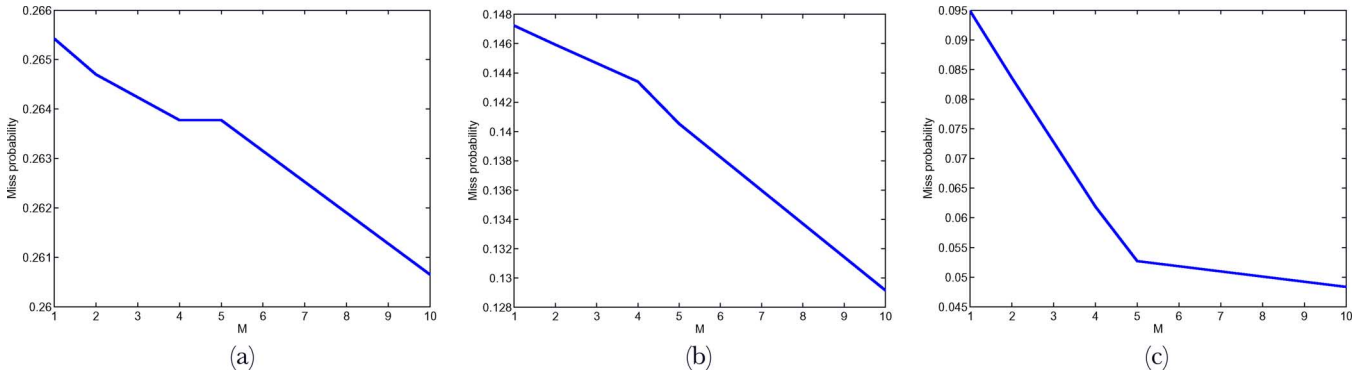

Fig. 12. P_M versus M ($|\mathcal{X}| = 1$, SNR $= -3$ dB): (a) $A = 0.1$; (b) $A = 1$; and (c) $A = 10$.

$M = 2$ is observed. In the highly correlated case $(A = 1)$, we see the maximal value of the error exponent at (0,0), (0,Δ),(Δ,0), and (Δ, Δ), which all correspond to periodic clustering. Hence, periodic clustering is the best among all configurations. In this case, it is seen that uniform configuration, i.e., $(x_2, x_3) = (\Delta/3, 2\Delta/3)$ or $(2\Delta/3, \Delta/3)$, is the worst configuration. As the field correlation becomes weak, however, the best configuration moves to uniform configuration eventually, as seen in Fig. 10(d). Interestingly, it is observed that placing two sensors clustered and one in the middle of the spatial period is optimal for transitory values of field correlation as shown in Fig. 10(b) and (c).

At low SNR, similar behavior to the case of $M = 2$ is observed, and the results confirm that periodic clustering gives the best configuration for most values of field correlations at low SNR.

IV. Simulations

In this section, we provide numerical results to verify our analytic results presented in the previous sections. Neyman–Pearson tests were used in all scenarios. The thresholds were chosen so that the false alarm probability was fixed at $\alpha = 1\%$. Note that our analysis is based on the error exponent that is the slope of the exponential error decay in large sample scheme, and the miss probability is approximately given by $P_M \approx Ce^{-nK}$ when the number of samples is large. Hence, the largest error exponent would result in the smallest error probability for a given number of observation samples in large sample scheme. In the simulations, we obtained the actual miss probability (or detection probability) to validate the analysis based on the error exponent in finite sample cases. Only a limited number of sensors are used, especially, in high SNR cases. This is because the detection probabilities of all the schemes are almost one and it is hard to see the performance difference if a large number of sensors are used in high SNR cases. We set the number of sensors as large as possible, as long as there is a meaningful result. It is seen that, even in the cases with very limited number of sensors $(n = 11)$, the simulation results still match the behavior predicted by the analysis based on the error exponent.

A. Uniform and Periodic Clustering Configuration

Fig. 11 shows the miss probability for different diffusion rates at 10-dB SNR. The total number of sensors is fixed to $n = 40$, and the cluster size is chosen as $M = [1, 2, 4, 5, 10]$. For the highly correlated field $(A = 0.1)$, it is observed that the reduced correlation between signal samples is the dominant factor and clustering $(M > 1)$ gives better performance than uniform configuration (i.e., $M = 1$). For the highly independent signal field $(A = 10)$, on the other hand, clustering yields worse performance than the uniform configuration. For the signal field with intermediate correlation, there is a tradeoff between the gain and loss of clustering, and there exists an optimal cluster size as shown in Fig. 11(b). The simulation results match the theoretically predicted behavior shown in Fig. 6.

Fig. 12 shows the miss probability for different diffusion rates at -3-dB SNR. The total number of sensors is fixed to $n = 100$,

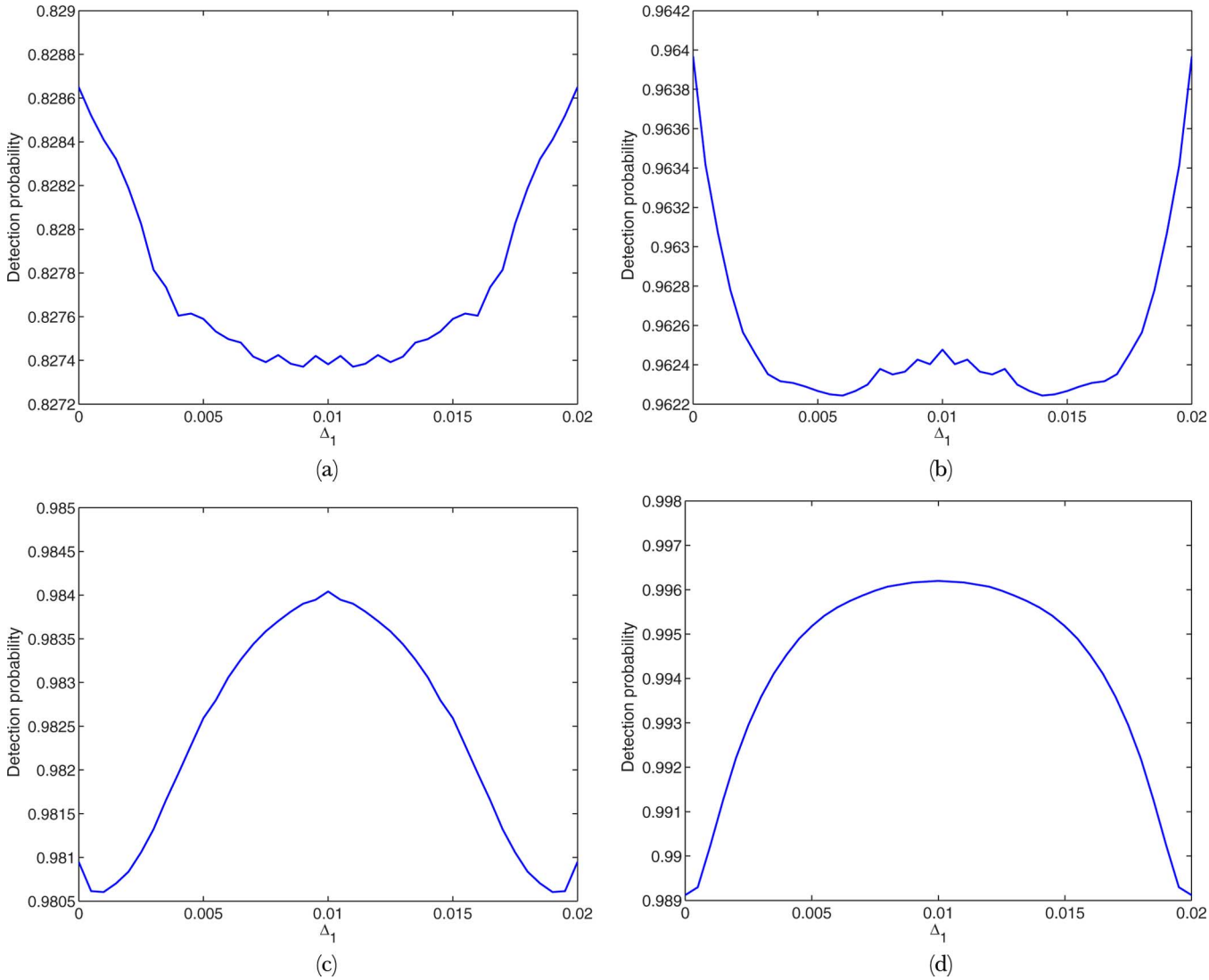

Fig. 13. P_D versus Δ_1 ($M = 2, \Delta = 0.02$, SNR $= 10$ dB): (a) $A = 1$; (b) $A = 15$; (c) $A = 30$; and (d) $A = 100$.

and the cluster size is chosen as $M = [1, 2, 4, 5, 10]$. It is seen that periodic clustering outperforms uniform configuration in all considered correlation values at -3-dB SNR, and the SNR is the dominant factor in the detector performance at low SNR. The simulation results here match the theoretical analysis shown in Fig. 7.

B. Arbitrary Periodic Configuration

We now investigate the detection performance for arbitrary periodic configuration. First, we consider the case of $M = 2$ in which we have the freedom to schedule one intermediate sensor at an arbitrary location within an interval $\Delta = 0.02$. Periodic clustering and uniform configuration are special cases of this configuration with $\Delta_1 = 0$ and $\Delta_1 = \Delta/2$, respectively.

Fig. 13 shows the detection probability $P_D (= 1 - P_M)$ as a function of the intermediate sensor location Δ_1 at high SNR. Here, $n = 11$ sensors are used. The locations of six sensors are fixed with a $\Delta = 0.02$ interval between adjacent ones, and the remaining five sensors are located in each of the five intervals, according to Δ_1. For the highly correlated field ($A = 1$), periodic clustering ($\Delta_1 = 0$) gives the best performance while the uniform configuration provides the worst. However, as the field correlation becomes weak ($A = 15$), we observe a second lobe growing at the uniform configuration point ($\Delta_1 = \Delta/2$). The value of the second lobe becomes larger than that corresponding to clustering as the correlation becomes weaker ($A = 30$), and eventually the detection probability decreases monotonically as the configuration deviates from uniform configuration to periodic clustering. This is consistent with the results using error exponents in the previous sections, as shown in Fig. 8.

Fig. 14 shows the detection probability for $M = 2$ at low SNR. $n = 101$ sensors are used. The locations of the sensors are set in a similar fashion as the setting in Fig. 13. It is seen that clustering is always the best strategy for all values of field correlation considered since the increase in the effective SNR due to noise averaging is the dominant factor in the detection performance at low SNR. It is also seen that the location of the

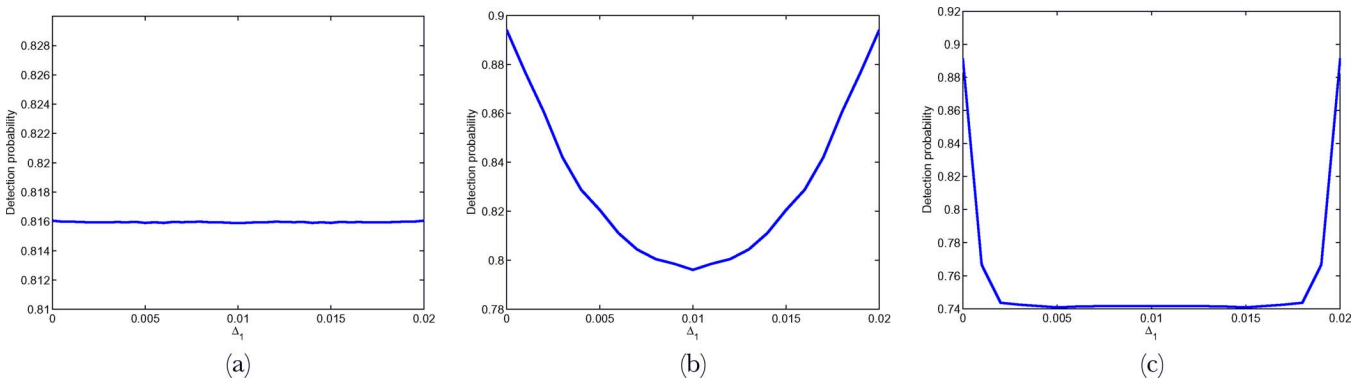

Fig. 14. P_D versus Δ_1 ($M = 2, \Delta = 0.02, \mathrm{SNR} = -3$ dB): (a) $A = 1$; (b) $A = 100$; and (c) $A = 1000$.

intermediate sensor is not important for the highly uncorrelated field $(A = 1000)$ unless it is very close to the first sensor within a period. This is consistent with the results using error exponents in the previous sections, as shown in Fig. 14. Note that the location of the intermediate sensor makes much less difference in highly correlated fields $(A = 1)$ than in highly uncorrelated fields ($A = 100$,1000).

Next, we consider the case of $M = 3$ in which we have freedom to schedule two intermediate sensors at an arbitrary location within an interval $\Delta = 0.03$. Fig. 15 shows the contour and surface of the detection probability as a function of the locations of the two intermediate sensors, with various field correlations. The SNR is set to 10 dB. Similar to the analysis of the error exponent in Section III, for the highly correlated signal field $(\mathrm{A} = 1)$, the best results are produced by periodic clustering, and the worst results are from a uniform configuration. As the field correlation becomes weak, the uniform configuration becomes the best scheme gradually. It is also seen that placing two sensors clustered and a third one in the middle of the spatial period is optimal for transitory values of signal field correlation, as shown in Fig. 15(b).

C. Uniform Configuration With Random Perturbation

Finally, the uniform configuration with random perturbation is studied. Eleven sensors are placed uniformly, at location $x_1 \cdots, x_{11}$ with an interval of $\Delta = 0.02$. Random perturbations are introduced to the 9 sensors in the middle, their locations are set to be $x_i' = x_i + \epsilon_i$, $i = 2, \cdots, 9$, where the ϵ_i's are independent and uniformly distributed on $(-\alpha\Delta, \alpha\Delta)$. In Fig. 16, α is set to be 0.1 or 0.5, corresponding to random perturbations being scaled by 10% or 50% of Δ. The uniform configuration and periodic clustering with $M = 2$ are also plotted. Both high SNR and low SNR cases are studied. It is seen in Fig. 16 that the performance of the uniform configuration with random perturbation is not much different from that of the uniform configuration in the high SNR case, whereas it is better than that of the uniform configuration in the low SNR case. When the sensor field covers the same spatial length, spatial perturbation makes some sensor spacing larger than that of the uniform case and other spacing less than that of the uniform case. When the SNR is high and the field correlation is weak, it can be shown that the total sum of Kullback–Leibler information is approximately given by the sum of per-sensor error exponent that is a monotone increasing concave function of the sensor spacing as shown in Fig. 4. In this case, the increase of the per-sensor error exponent due to the enlarged spacing cannot compensate for the error exponent decrease due to the reduced sensor spacing, and thus the perturbation yields worse performance. When the SNR is low, however, the perturbation provides clustered sensors and this clustering provides a benefit to the performance, as shown in Fig. 16(b).

V. Conclusion

We have considered energy-efficient sensor selection for large sensor networks deployed to detect correlated random fields. Using our previous results on the error exponent in Neyman–Pearson detection, we have analyzed and compared the detection capabilities of different sensor configuration strategies in the large sample regime. The optimal configuration is a function of the field correlation and the SNR of sensor observations. For the uniform configuration, the activated sensors should be maximally separated to cover the entire signal field at high SNR, whereas at low SNR there exists an optimal spacing between the activated sensors. We have also provided the error exponents of periodic clustering and arbitrary periodic configurations. Depending on the field correlation and SNR, periodic clustering may outperform the uniform configuration. Furthermore, there exists an optimal cluster size for intermediate values of correlation. The closed-form error exponent obtained for the vector state-space model explains the transitory behavior of the optimal scheme from periodic clustering to the uniform configuration as the field correlation changes. Simulations confirm the validity of our analysis using asymptotic results for finite sample sizes. Throughout the paper, we have assumed that sensors have already been deployed over the field and considered the activation for sensing and transmission from the selected sensors. The results here are also applicable to sensor placement problem where n sensors are to be deployed over a signal field for a detection application.

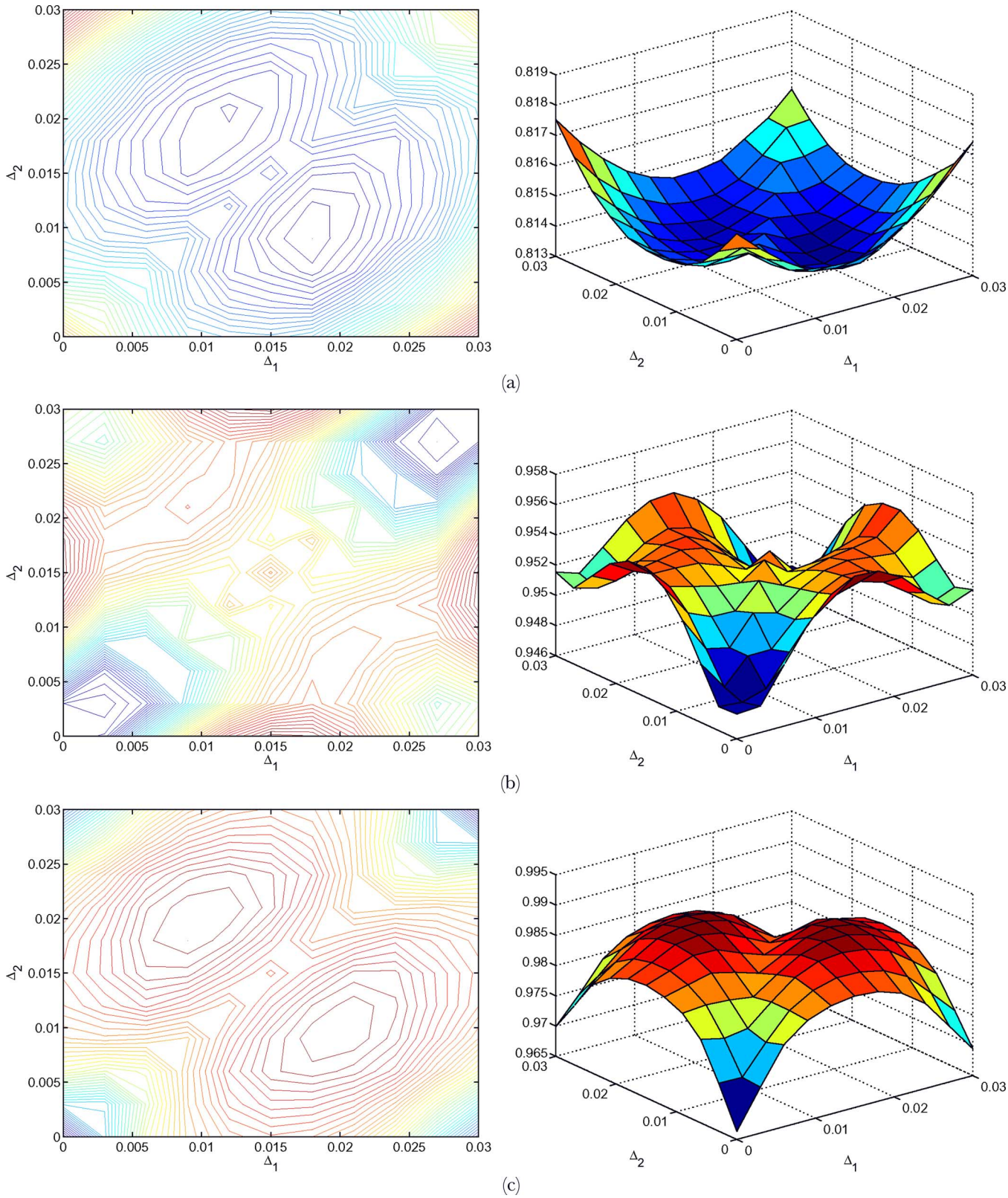

Fig. 15. P_D versus Δ_1 and Δ_2 ($M = 3$, $\Delta = 0.03$, SNR $= 10$ dB): (a) $A = 1$; (b) $A = 16$; and (c) $A = 50$.

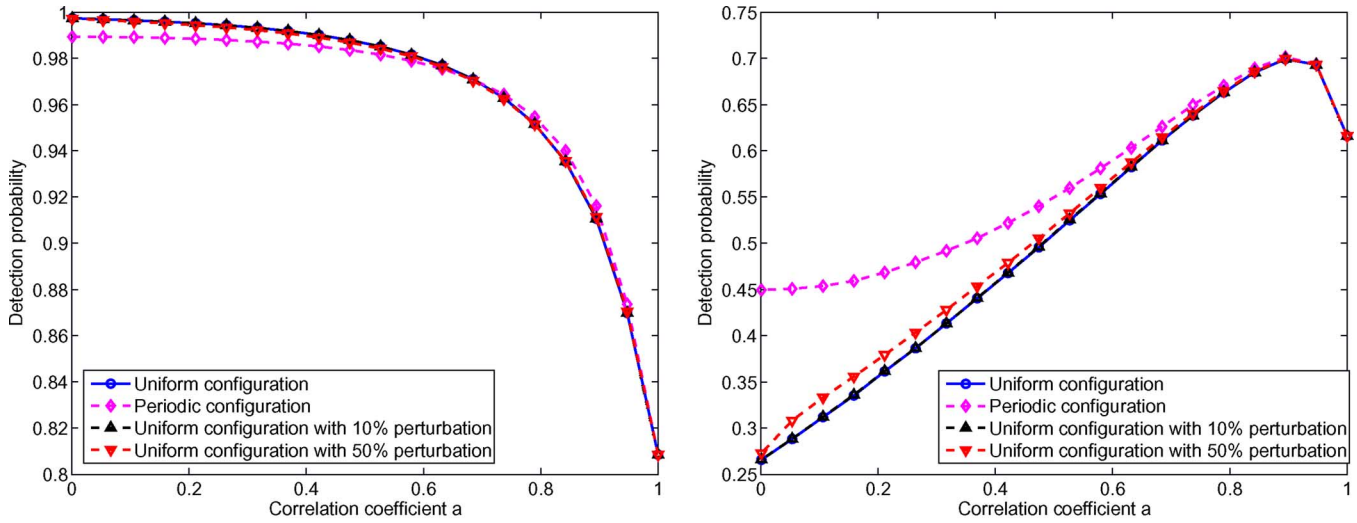

Fig. 16. P_D versus correlation coefficient a: (a) SNR $=$ 10 dB and (b) SNR $=-6$ dB.

APPENDIX

A. Proof of Proposition 1

For two distributions $p_{0,n}(\mathbf{y}_n) = \mathcal{N}(\mathbf{0}, \boldsymbol{\Sigma}_{0,n})$ and $p_{1,n}(\mathbf{y}_n) = \mathcal{N}(\mathbf{0}, \boldsymbol{\Sigma}_{1,n})$, the error exponent is given by the almost-sure limit of the Kullback–Leibler rate

$$\frac{1}{n}\log\frac{p_{0,n}}{p_{1,n}}(\mathbf{y}_n) = \frac{1}{n}\left(\frac{1}{2}\log\left(\frac{\det(\boldsymbol{\Sigma}_{1,n})}{\det(\boldsymbol{\Sigma}_{0,n})}\right) - \frac{1}{2}\mathbf{y}_n^T\left(\boldsymbol{\Sigma}_{0,n}^{-1} - \boldsymbol{\Sigma}_{1,n}^{-1}\right)\mathbf{y}_n\right) \quad (33)$$

under $p_{0,n}$ [12]. Here, $p_{0,n}$ and $p_{1,n}$ denote the probability density of $\mathbf{y}_n$ under H_0 and H_1, respectively.

Let the eigendecomposition of $\boldsymbol{\Sigma}_{s,N}(\tilde{a})$ be $\boldsymbol{\Sigma}_{s,N}(\tilde{a}) = \mathbf{U}\boldsymbol{\Lambda}\mathbf{U}^T$, where $\boldsymbol{\Lambda} = \mathrm{diag}(\lambda_1, \lambda_2, \cdots, \lambda_N)$ and $\tilde{a} = e^{-A\tilde{\Delta}}$. Then, by the properties of the Kronecker product we have $\boldsymbol{\Sigma}_{s,N}(\tilde{a}) \otimes \mathbf{1}_M\mathbf{1}_M^T = \tilde{\mathbf{U}}\tilde{\boldsymbol{\Lambda}}\tilde{\mathbf{U}}^T$, where $\tilde{\boldsymbol{\Lambda}} = \mathrm{diag}(M\lambda_1, 0, \cdots, 0, M\lambda_2, 0, \cdots, 0, M\lambda_N, 0, \cdots, 0)$, (Here, we have N nonzero elements and $(M-1)N$ zero elements.) and $\tilde{\mathbf{u}}_{(i-1)M+1} = \mathbf{u}_i \otimes (1/\sqrt{M})\mathbf{1}_M$, $i = 1, 2, \cdots, N$. Here, $\mathbf{u}_i$ and $\tilde{\mathbf{u}}_j$ are the ith and jth column vectors of $\mathbf{U}$ and $\tilde{\mathbf{U}}$, respectively. The covariance matrices under H_1 and H_0 are given by $\boldsymbol{\Sigma}_{1,n} = \tilde{\mathbf{U}}(\tilde{\boldsymbol{\Lambda}} + \sigma^2\mathbf{I})\tilde{\mathbf{U}}^T$ and $\boldsymbol{\Sigma}_{0,n} = \sigma^2\tilde{\mathbf{U}}\tilde{\mathbf{U}}^T$ Thus, we have $\det(\boldsymbol{\Sigma}_{1,n})/\det(\boldsymbol{\Sigma}_{0,n}) = \prod_{i=1}^{N}(M\lambda_i + \sigma^2/\sigma^2$. Using the asymptotic distribution of the eigenvalues of a Toeplitz matrix [16], [17], we have

$$\lim_{n\to\infty}\frac{1}{n}\log\frac{\det(\boldsymbol{\Sigma}_{1,n})}{\det(\boldsymbol{\Sigma}_{0,n})} = \frac{1}{2\pi M}\int_0^{2\pi}\log\frac{MS_s(\omega)+\sigma^2}{\sigma^2}d\omega \quad (34)$$

where $S_s(\omega)$ is the spectrum of the signal sample at locations $\{i\tilde{\Delta}, i = 0, 1, 2, \cdots\}$ which has finite lower and upper bounds.

For the second term in the right-hand side of (33), we have

$$\boldsymbol{\Sigma}_{0,n}^{-1} - \boldsymbol{\Sigma}_{1,n}^{-1} = \tilde{\mathbf{U}}\mathrm{diag}\left(\frac{M\lambda_1}{\sigma^2(M\lambda_1+\sigma^2)}, 0, \cdots, 0, \frac{M\lambda_2}{\sigma^2(M\lambda_2+\sigma^2)}, 0, \cdots, \frac{M\lambda_N}{\sigma^2(M\lambda_N+\sigma^2)}, 0, \cdots, 0\right)\tilde{\mathbf{U}}^T$$

and

$$\mathbf{y}_n^T\left(\boldsymbol{\Sigma}_{0,n}^{-1} - \boldsymbol{\Sigma}_{1,n}^{-1}\right)\mathbf{y}_n = \tilde{\mathbf{y}}_n^T\mathbf{U}\left(\frac{M\lambda_1}{\sigma^2(M\lambda_1+\sigma^2)}, \frac{M\lambda_2}{\sigma^2(M\lambda_2+\sigma^2)}, \cdots, \frac{M\lambda_N}{\sigma^2(M\lambda_N+\sigma^2)}\right)\mathbf{U}^T\tilde{\mathbf{y}}_n$$

where

$$\tilde{\mathbf{y}}_n = \left[(1/\sqrt{M})\sum_{i=1}^{M} y_i, (1/\sqrt{M})\sum_{i=M+1}^{2M} y_i, \cdots, (1/\sqrt{M})\sum_{i=(N-1)M+1}^{MN} y_i\right].$$

The limiting behavior of $n^{-1}\mathbf{y}_n^T(\boldsymbol{\Sigma}_{0,n}^{-1} - \boldsymbol{\Sigma}_{1,n}^{-1})\mathbf{y}_n$ is also known and is given by

$$\lim_{n\to\infty}\frac{1}{n}\mathbf{y}_n^T\left(\boldsymbol{\Sigma}_{0,n}^{-1} - \boldsymbol{\Sigma}_{1,n}^{-1}\right)\mathbf{y}_n = \frac{1}{2\pi M}\int_0^{2\pi}\frac{MS_s(\omega)}{MS_s(\omega)+\sigma^2}d\omega \quad (35)$$

where the limit is in the almost-sure sense convergence under H_0, provided that $S_s(\omega)$ is continuous and strictly positive [18]. Combining (33), (34), and (35) gives

$$K = \frac{1}{M}\frac{1}{2\pi}\int_0^{2\pi}\left(\frac{1}{2}\log\frac{MS_s(\omega)+\sigma^2}{\sigma^2} - \frac{1}{2}\frac{MS_s(\omega)}{MS_s(\omega)+\sigma^2}\right)d\omega, \quad (36)$$

and

$$(1/2\pi)\int_0^{2\pi}\{(1/2)\log[(S_s(\omega)+\sigma^2)/\sigma^2] - (1/2)S_s(\omega)/(S_s(\omega)+\sigma^2)\}d\omega$$

is the error exponent in Theorem 1 in the spectral domain. This concludes the proof. Note that the error exponent is $1/M$ times that of the uniform configuration with the signal power increased M-fold. ■

B. Comments on Theorem 1 and Proposition 1

Since the uniform configuration and periodic clustering are special cases of arbitrary periodic configuration, Theorem 1 and Proposition 1 can also be obtained by applying Proposition 2. The uniform case is straightforward. In case of periodic clustering, $\mathbf{A} = \tilde{a}[\mathbf{O}; \mathbf{1}_M]$, ($\mathbf{O}$ is a matrix with all zero elements), $\mathbf{B}$ is a lower triangular matrix with all diagonal and lower diagonal elements being one, and $\mathbf{Q} = \Pi_0 \mathrm{diag}[(1-\tilde{a}^2), 0, \cdots, 0]$. Solving the Riccati (30) and Lyapunov (32) yields

$$\mathbf{P} = \mathbf{U}\mathrm{diag}(P_1, 0, \cdots, 0)\mathbf{U}^T, \quad \tilde{\mathbf{P}} = \mathbf{U}\mathrm{diag}(P_2, 0, \cdots, 0)\mathbf{U}^T$$

where $\mathbf{U}$ is a unitary matrix of which first column is $(1/\sqrt{M})[1, \cdots, 1]^T$, P_1 is the solution of the scalar Riccati equation with signal power $M\Pi_0$, and P_2 is the solution of the scalar Lyapunov equation corresponding to P_1, i.e., $P_2 = (\tilde{a} - (\tilde{a}P_1/\sigma^2 + P_1))^2 P_2 + (\tilde{a}P_1/\sigma^2 + P_1)^2$. Hence, we have

$$\begin{aligned}\mathbf{R}_e &= \mathbf{U}\mathrm{diag}(\sigma^2 + P_1, \sigma^2, \cdots, \sigma^2)\mathbf{U}^T \\ \tilde{\mathbf{R}}_e &= \sigma^2 \mathbf{U}\mathrm{diag}(1 + P_2, 1, \cdots, 1)\mathbf{U}^T.\end{aligned}$$

From (28), the per-cluster error exponent K_v is given by

$$\begin{aligned}K_v &= -\frac{1}{2}\log\frac{\sigma^{2M}}{(\sigma^2+P_1)\sigma^{2(M-1)}} \\ &\quad + \frac{1}{2}\mathrm{tr}\left(\mathrm{diag}\left(\frac{1}{\sigma^2+P_1}, \frac{1}{\sigma^2}, \cdots, \frac{1}{\sigma^2}\right)\right. \\ &\qquad \left.\times \mathrm{diag}\left(\sigma^2(1+P_2), \sigma^2, \cdots, \sigma^2\right)\right) - \frac{M}{2}, \\ &= -\frac{1}{2}\log\frac{\sigma^2}{\sigma^2+P_1} + \frac{1}{2}\frac{\sigma^2(1+P_2)}{\sigma^2+P_1} + \frac{M-1}{2} - \frac{M}{2} \\ &= -\frac{1}{2}\log\frac{\sigma^2}{R_e} + \frac{1}{2}\frac{\tilde{R}_e}{R_e} - \frac{1}{2}.\end{aligned}$$

This is the error exponent in (8) with the signal power given by $M\Pi_0$ and needs to be scaled by $1/M$ for the per-sensor error exponent.

C. Proof of Proposition 2

The proof is similar to that in [2], where the scalar observation process is considered. Here, we extend to the vector observation process case. The error exponent is given by the almost-sure limit of the normalized LLR $(1/n)\log L_n(Y_n)$ under H_0, where $Y_n = \{\vec{y}_i\}_{i=1}^n$. The LLR is given by

$$\log L_n(Y_n) = \log p_{1,n}(Y_n) - \log p_{0,n}(Y_n). \tag{37}$$

Under H_0, the elements of Y_n are i.i.d. zero-mean Gaussian with variance σ^2. We have

$$p_{0,n}(Y_n) = (2\pi\sigma^2)^{nM/2} \exp\left\{-\frac{1}{2\sigma^2}\sum_{i=1}^n \vec{y}_i^T\vec{y}_i\right\}. \tag{38}$$

So

$$\begin{aligned}\frac{1}{n}\log p_{0,n}(Y_n) &= -\frac{M}{2}\log(2\pi\sigma^2) - \frac{1}{2\sigma^2}\frac{1}{n}\sum_{i=1}^n \vec{y}_i^T\vec{y}_i \\ &\to -\frac{M}{2}\log(2\pi\sigma^2) - \frac{M}{2} \quad \text{a.s.}\end{aligned} \tag{39}$$

since $(1/n)\sum_{i=1}^n \vec{y}_i^T\vec{y}_i \to \mathbb{E}[\vec{y}_i^T\vec{y}_i] = M\sigma^2$, almost surely (a.s.) under H_0, as $n \to \infty$, by SLLN.

Now, let us focus on $(1/n)\log p_{1,n}(Y_n)$. Define $l_i = \log p_{1,i}(\vec{y}_1^i)$, where $\vec{y}_1^i = \{\vec{y}_1, \vec{y}_2, \cdots, \vec{y}_i\}$. Since

$$p_{1,i}\left(\vec{y}_1^i\right) = p_{1,i-1}\left(\vec{y}_1^{i-1}\right) p_{1,i|i-1}\left(\vec{y}_i|\vec{y}_1^{i-1}\right) \tag{40}$$

and $p_{1,i|i-1}(\vec{y}_i|\vec{y}_1^{i-1}) = \mathcal{N}(\hat{\vec{y}}_{i|i-1}, \mathbf{R}_{e,i})$, we have

$$l_i = l_{i-1} + \log p_{1,i|i-1}\left(\vec{y}_i|\vec{y}_1^{i-1}\right) \tag{41}$$

$$= l_{i-1} - \frac{1}{2}\log|2\pi\mathbf{R}_{e,i}| - \frac{1}{2}\vec{e}_i^T\mathbf{R}_{e,i}^{-1}\vec{e}_i \tag{42}$$

where $\vec{e}_i \triangleq \vec{y}_i - \hat{\vec{y}}_{i|i-1}$, which is also known as the innovation with covariance matrix $\mathbf{R}_{e,i} = \mathbb{E}_1\{\vec{e}_i\vec{e}_i^T\}$. Hence

$$\begin{aligned}\frac{1}{n}\log p_{1,n}(Y_n) &= \frac{l_n}{n} \\ &= -\frac{M}{2}\log(2\pi) - \frac{1}{2n}\sum_{i=1}^n \log|\mathbf{R}_{e,i}| \\ &\quad - \frac{1}{2n}\sum_{i=1}^n \vec{e}_i^T\mathbf{R}_{e,i}^{-1}\vec{e}_i.\end{aligned} \tag{43}$$

The second term on the right-hand side of (44) is not random, and we have

$$\frac{1}{2n}\sum_{i=1}^n \log|\mathbf{R}_{e,i}| \to \frac{1}{2}\log|\mathbf{R}_e| \tag{44}$$

by the Cesáro mean theorem, since $\mathbf{R}_{e,i}$ is a finite-dimension matrix, $\mathbf{R}_{e,i} \to \mathbf{R}_e$ and $\mathbf{R}_{e,i} \geq \sigma^2\mathbf{I} \geq \mathbf{0}$, where $\mathbf{A} \geq \mathbf{B}$ means $\mathbf{A} - \mathbf{B}$ is positive semidefinite. $\mathbf{R}_e$ is given by

$$\mathbf{R}_e = \sigma^2\mathbf{I} + \mathbf{P} \tag{45}$$

where $\mathbf{P}$ is the stead-state error covariance of the one-step predictor for the signal $\{\vec{s}_i\}$ and is given by the unique stabilizing solution of the distrete-time Riccati equation

$$\mathbf{P} = \mathbf{A}\mathbf{P}\mathbf{A}^T + \mathbf{B}\mathbf{Q}\mathbf{B}^T - \mathbf{A}\mathbf{P}\mathbf{R}_e^{-1}\mathbf{P}\mathbf{A}^T \tag{46}$$

such that $\mathbf{A} - \mathbf{K}_p$ is stable (the existence of the solution is guaranteed since $\mathbf{A}$ is stable and $\mathrm{diag}(\mathbf{B}\mathbf{Q}\mathbf{B}^T, \sigma^2\mathbf{I}) \geq 0$; see [2]), and $\mathbf{K}_p = \mathbf{A}\mathbf{P}\mathbf{R}_e^{-1}$ is the stead-state Kalman prediction gain.

Consider the third term of the right-hand side (RHS) of (43). The innovation process $\vec{e}_i$ is a sequence of random vectors, and given by a linear combination of $\{\vec{y}_1, \vec{y}_2, \cdots, \vec{y}_i\}$, i.e.,

$$\begin{aligned}\vec{e}_i &= \vec{y}_i - \mathbf{K}_{p,i-1}\vec{y}_{i-1} - [\mathbf{A} - \mathbf{K}_{p,i-1}]\mathbf{K}_{p,i-2}\vec{y}_{i-2} \\ &\quad - [\mathbf{A} - \mathbf{K}_{p,i-1}][\mathbf{A} - \mathbf{K}_{p,i-2}]\mathbf{K}_{p,i-3}\vec{y}_{i-3} - \cdots.\end{aligned} \tag{47}$$

Here, $\mathbf{K}_{p,i} \triangleq \mathbf{A}\mathbf{P}_i\mathbf{R}_{e,i}^{-1}$ is the Kalman predition gain, $\mathbf{P}_i \triangleq \mathbb{E}\{(\vec{s}_i - \hat{\vec{s}}_{i|i-1})^2\}$ is the error covariance at time i, and $\hat{\vec{s}}_{i|i-1}$ is the LMMSE prediction of $\vec{s}_i$ given $\vec{y}_1^{i-1}$. Since the Kalman filter

converges asymptotically to the time-invariant recursive Wiener filter for a stable $\mathbf{A}$, we have asymptotically

$$\vec{e}_i = \vec{y}_i - \mathbf{K}_p\vec{y}_{i-1} - [\mathbf{A}-\mathbf{K}_p]\mathbf{K}_p\vec{y}_{i-2} - [\mathbf{A}-\mathbf{K}_p]^2\mathbf{K}_p\vec{y}_{i-3} - \cdots. \tag{48}$$

Under H_0, the sequence $\vec{y}_1^i$ is i.i.d. Gaussian, and the innovations sequence is the output of a stable recursive filter driven by $\vec{y}_1^i$. Since ergodicity holds for any vector stationary Gaussian process with continuous spectral distribution function [3], it is easy to see that the sequence $\{\vec{e}_i\}$ is ergodic. By the ergodic theorem, $(1/n)\sum_{i=1}^n \vec{e}_i\vec{e}_i^T$ converges to its true expectation given by

$$\frac{1}{n}\sum_{i=1}^{n}\vec{e}_i\vec{e}_i^T \to \tilde{\mathbf{R}}_e \triangleq \mathbb{E}_0\left\{\vec{e}_i\vec{e}_i^T\right\}, \tag{49}$$

and $\tilde{\mathbf{R}}_e$ is given by

$$\tilde{\mathbf{R}}_e = \sigma^2\left(\mathbf{I}_M + \sum_{i=0}^{\infty}[\mathbf{A}-\mathbf{K}_p]^i\mathbf{K}_p\mathbf{K}_p^T\left[\mathbf{A}^T-\mathbf{K}_p^T\right]^i\right). \tag{50}$$

Define

$$\tilde{\mathbf{P}} \triangleq \sum_{i=0}^{\infty}[\mathbf{A}-\mathbf{K}_p]^i\mathbf{K}_p\mathbf{K}_p^T\left[\mathbf{A}^T-\mathbf{K}_p^T\right]^i. \tag{51}$$

Since $\mathbf{A}-\mathbf{K}_p$ is stable, the series convergences absolutely to a finite matrix, which is given by the following Lyapunov equation [2]:

$$\tilde{\mathbf{P}} = (\mathbf{A}-\mathbf{K}_p)\tilde{\mathbf{P}}(\mathbf{A}-\mathbf{K}_p)^T + \mathbf{K}_p\mathbf{K}_p^T. \tag{52}$$

Now, the third term on the RHS of (43) can be rewritten as

$$\begin{aligned}\frac{1}{2n}\sum_{i=1}^{n}\vec{e}_i^T\mathbf{R}_{e,i}^{-1}\vec{e}_i &= \frac{1}{2n}\sum_{i=1}^{n}\mathrm{tr}\left(\mathbf{R}_{e,i}^{-1}\vec{e}_i\vec{e}_i^T\right)\\ &= \mathrm{tr}\left(\frac{1}{2n}\sum_{i=1}^{n}\mathbf{R}_{e,i}^{-1}\vec{e}_i\vec{e}_i^T\right).\end{aligned} \tag{53}$$

It is known that $\mathbf{R}_{e,i}$ converges to $\mathbf{R}_e$ exponentially [2]. Hence, we have $\mathbf{R}_{e,i} = \mathbf{R}_e + C_1\epsilon^i\mathbf{1}\mathbf{1}^T$ for some $|\epsilon| < 1$ and by applying the matrix inversion lemma

$$\begin{aligned}\mathbf{R}_{e,i}^{-1} &= (\mathbf{R}_e + C_1\epsilon^i\mathbf{1}\mathbf{1}^T)^{-1},\\ &= \mathbf{R}_e^{-1} - \mathbf{R}_e^{-1}\mathbf{1}\left(C_1^{-1}\epsilon^{-i} + \mathbf{1}^T\mathbf{R}_e^{-1}\mathbf{1}\right)^{-1}\mathbf{1}^T\mathbf{R}_e^{-1} &(54)\\ &= \mathbf{R}_e^{-1} - \left(C_1^{-1}\epsilon^{-i} + \mathbf{1}^T\mathbf{R}_e^{-1}\mathbf{1}\right)^{-1}\mathbf{R}_e^{-1}\mathbf{1}\mathbf{1}^T\mathbf{R}_e^{-1} &(55)\\ &= \mathbf{R}_e^{-1} - \frac{C_1\epsilon^i}{1+C_2\epsilon^i}\mathbf{R}_e^{-1}\mathbf{1}\mathbf{1}^T\mathbf{R}_e^{-1} &(56)\end{aligned}$$

where $C_1 > 0$ and C_2 are some constants. Substituting this into (53) yields

$$\begin{aligned}&\mathrm{tr}\left(\frac{1}{2n}\sum_{i=1}^{n}\mathbf{R}_{e,i}^{-1}\vec{e}_i\vec{e}_i^T\right)\\ &\quad= \mathrm{tr}\left(\frac{1}{2n}\sum_{i=1}^{n}\left(\mathbf{R}_e^{-1} - \frac{C_1\epsilon^i}{1+C_2\epsilon^i}\mathbf{R}_e^{-1}\mathbf{1}\mathbf{1}^T\mathbf{R}_e^{-1}\right)\vec{e}_i\vec{e}_i^T\right)\\ &\quad= \mathrm{tr}\left(\frac{1}{2n}\sum_{i=1}^{n}\mathbf{R}_e^{-1}\vec{e}_i\vec{e}_i^T\right)\\ &\qquad- \mathrm{tr}\left(\frac{1}{2n}\sum_{i=1}^{n}\left(\frac{C_1\epsilon^i}{1+C_2\epsilon^i}\mathbf{R}_e^{-1}\mathbf{1}\mathbf{1}^T\mathbf{R}_e^{-1}\right)\vec{e}_i\vec{e}_i^T\right)\\ &\quad= \mathrm{tr}\left(\mathbf{R}_e^{-1}\frac{1}{2n}\sum_{i=1}^{n}\vec{e}_i\vec{e}_i^T\right)\\ &\qquad- \mathrm{tr}\left(\mathbf{R}_e^{-1}\mathbf{1}\mathbf{1}^T\mathbf{R}_e^{-1}\frac{1}{2n}\sum_{i=1}^{n}\frac{C_1\epsilon^i}{1+C_2\epsilon^i}\vec{e}_i\vec{e}_i^T\right).\end{aligned} \tag{57}$$

The first term converges to $(1/2)\mathrm{tr}(\mathbf{R}_e^{-1}\tilde{\mathbf{R}}_e)$, and the second term converges to zero since $(1/n)\sum_{i=1}^n\vec{e}_i\vec{e}_i^T$ converges to a matrix with a finite elements. Combining (39), (43) and (44) with the above, we have

$$\begin{aligned}K &= -\lim_{n\to\infty}\frac{1}{n}\frac{\log p_{1,n}(Y_n)}{\log p_{0,n}(Y_n)}\\ &= \left(-\frac{1}{2}\log(\sigma^{2M}) - \frac{M}{2}\right)\\ &\quad- \left(-\frac{1}{2}\log|\mathbf{R}_e| - \frac{1}{2}\mathrm{tr}\left(\mathbf{R}_e^{-1}\tilde{\mathbf{R}}_e\right)\right)\\ &= -\frac{1}{2}\log\frac{\sigma^{2M}}{|\mathbf{R}_e|} + \frac{1}{2}\mathrm{tr}\left(\mathbf{R}_e^{-1}\tilde{\mathbf{R}}_e\right) - \frac{M}{2}.\end{aligned}$$

■

REFERENCES

[1] H. V. Poor, *An Introduction to Signal Detection and Estimation*, 2nd ed. New York: Springer, 1994.

[2] Y. Sung, L. Tong, and H. V. Poor, "Neyman–Pearson detection of Gauss–Markov signals in noise: Closed-form error exponent and properties," *IEEE Trans. Inf. Theory*, vol. 52, no. 4, pp. 1354–1365, Apr. 2006.

[3] Y. Sung, L. Tong, and H. V. Poor, "Sensor configuration and activation for field detection in large sensor arrays," presented at the 2005 Information Processing in Sensor Networks (IPSN), Los Angeles, CA, Apr. 2005.

[4] T. Kailath and H. V. Poor, "Detection of stochastic processes," *IEEE Trans. Inf. Theory*, vol. 44, no. 6, pp. 2230–2259, Oct. 1998.

[5] G. R. Benitz and J. A. Bucklew, "Large deviation rate calculations for nonlinear detectors in Gaussian noise," *IEEE Trans. Inf. Theory*, vol. 36, no. 2, pp. 358–371, Mar. 1990.

[6] R. K. Bahr, "Asymptotic analysis of error probabilities for the nonzero-mean Gaussian hypothesis testing problem," *IEEE Trans. Inf. Theory*, vol. 36, no. 3, pp. 597–607, Mar. 1990.

[7] R. K. Bahr and J. A. Bucklew, "Optimal sampling schemes for the Gaussian hypothesis testing problem," *IEEE Trans. Acoust., Speech, Signal Process.*, vol. 38, no. 10, pp. 1677–1686, Oct. 1990.

[8] P. Barone, A. Gigli, and M. Piccioni, "Optimal importance sampling for some quadratic forms of ARMA processes," *IEEE Trans. Inf. Theory*, vol. 41, no. 6, pp. 1834–1844, Nov. 1995.
[9] W. Bryc and W. Smolenski, "On the large deviation principle for a quadratic functional of the autoregressive process," *Stat. Probab. Lett.*, vol. 17, pp. 281–285, 1993.
[10] B. Bercu, F. Gamboa, and A. Rouault, "Large deviations for quadratic forms of stationary Gaussian processes," *Stoch. Process. Appl.*, vol. 71, pp. 75–90, 1997.
[11] H. Luschgy, "Asymptotic behavior of Neyman–Pearson tests for autoregressive processes," *Scand. J. Stat.*, vol. 21, pp. 461–473, 1994.
[12] R. R. Bahadur, S. L. Zabell, and J. C. Gupta, "Large Deviations, Tests, and Estimates," in *Asymptotic Theory of Statistical Tests and Estimation: In Honor of Wassily Hoeffding*, I. M. Chakravarti, Ed. New York: Academic, 1980.
[13] F. C. Schweppe, "Evaluation of likelihood functions for Gaussian signals," *IEEE Trans. Inf. Theory*, vol. IT-11, no. 1, pp. 61–70, Jan. 1965.
[14] J.-F. Chamberland and V. V. Veeravalli, "Design of sensor networks for detection applications via large-deviation theory," presented at the 2004 IEEE Information Theory Workshop, San Antonio, TX, Oct. 2004.
[15] M. Micheli and M. I. Jordan, "Random sampling of a continuous-time stochastic dynamical system," presented at the 15th Int. Symp. Mathematical Theory of Networks and Systems (MTNS), Univ. Notre Dame, South Bend, IN, Aug. 2002, .
[16] U. Grenander and G. Szegö, *Toeplitz Forms and Their Applications*. Berkeley, CA: Univ. of California Press, 1958.
[17] R. Gray, "On the asymptotic eigenvalue distribution of Toeplitz matrices," *IEEE Trans. Inf. Theory*, vol. 18, no. 6, pp. 725–730, Nov. 1972.
[18] P. J. Brockwell and R. A. Davis, *Time Series: Theory and Methods*, 2nd ed. New York: Springer, 1991.

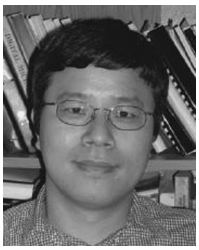

Youngchul Sung (S'92–M'95) received the B.S. and M.S. degrees in electronics engineering from Seoul National University, Seoul, Korea, in 1993 and 1995, respectively, and the Ph.D. degree in electrical engineering from Cornell University, Ithaca, NY, in 2005.

From 2005 until 2007, he worked as a Senior Engineer in the Corporate R & D Center in Qualcomm, Inc., San Diego, CA. Currently, he is an Assistant Professor in the Department of Electrical Engineering in the Korea Advanced Institute of Science and Technology (KAIST), Daejeon. His research interests include communication theory, statistical signal processing and their applications to wireless communication systems and related areas.

Xin Zhang (S'01–M'06) received the B.S. and M.S. degree in electrical engineering from Fudan University, Shanghai, China, in 1997 and 2000, respectively, and the Ph.D. degree from the Department of Electrical and Computer Engineering at the University of Connecticut, Storrs, in 2005.

From 2005 to 2006, he was a Postdoctoral Fellow at Princeton University, Princeton, NJ. Currently, he is with the United Technologies Research Center, East Hartford, CT. His research interests include wireless sensor networks, statistical signal processing, detection, and target tracking.

Lang Tong (S'87–M'91–SM'01–F'05) received the B.E. degree from Tsinghua University, Beijing, China, in 1985 and the M.S. and Ph.D. degrees in electrical engineering from the University of Notre Dame, Notre Dame, IN, in 1987 and 1991, respectively.

Currently, he is a Professor in the School of Electrical and Computer Engineering, Cornell University, Ithaca, NY.

Dr. Tong received the Young Investigator Award from the Office of Naval Research in 1996, the Outstanding Young Author Award from the IEEE Circuits and Systems Society, the 2004 Best Paper Award (with M. Dong) from the IEEE Signal Processing Society, and the 2005 Leonard G. Abraham Prize Paper Award (with P. Venkitasubramaniam and S. Adireddy) from the IEEE Communications Society.

H. Vincent Poor (S'72–M'77–SM'82–F'87) received the Ph.D. degree in electrical engineering and computer science from Princeton University, Princeton, NJ, in 1977.

From 1977 to 1990, he was on the faculty of the University of Illinois at Urbana-Champaign. Since 1990, he has been on the faculty at Princeton, where he is the Michael Henry Strater University Professor of Electrical Engineering and Dean of the School of Engineering and Applied Science. His research interests are in the areas of stochastic analysis, statistical signal processing, and their applications in wireless networks and related fields. Among his publications in these areas is the recent book *MIMO Wireless Communications* (Cambridge, U.K.: Cambridge Univ. Press, 2007).

Dr. Poor is a member of the National Academy of Engineering, a Fellow of the American Academy of Arts and Sciences, and a former Guggenheim Fellow. He is also a Fellow of the Institute of Mathematical Statistics, the Optical Society of America (OSA), and other organizations. In 1990, he served as President of the IEEE Information Theory Society, and from 2004 to 2007, he served as the Editor-in-Chief of the IEEE TRANSACTIONS ON INFORMATION THEORY. Recent recognition of his work includes the 2005 IEEE Education Medal and the 2007 IEEE Marconi Prize Paper Award.